A role for the subthalamic nucleus in aversive learning

Gian Pietro Serra, Adriane Guillaumin, Bianca Vlcek, Lorena Delgado-Zabalza, Alessia Ricci, Eleonora Rubino, Sylvie Dumas, Jérôme Baufreton, François Georges, Åsa Wallén-Mackenzie

Cell Reports

Article

A role for the subthalamic nucleus in aversive learning

Graphical abstract

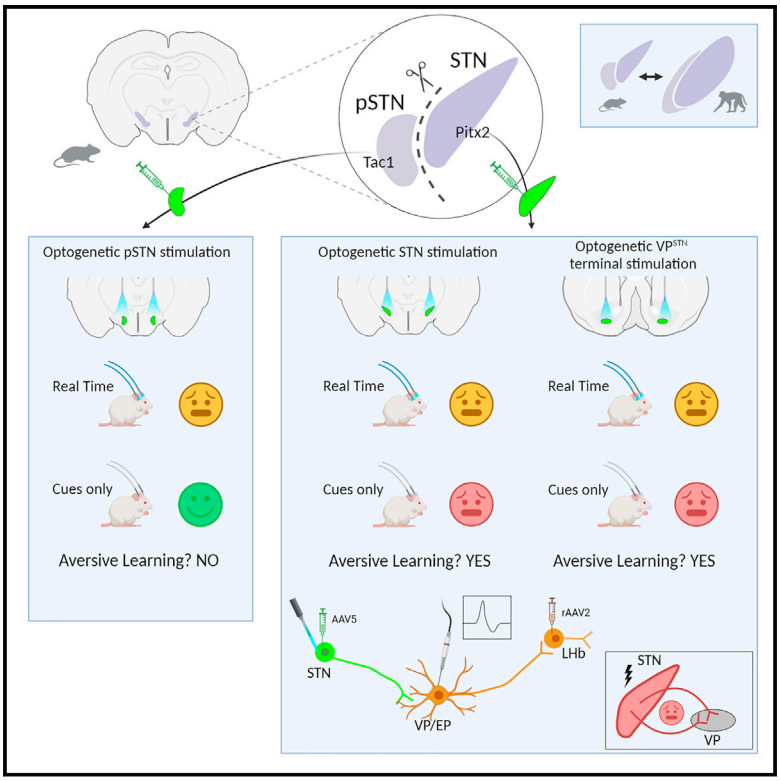

Highlights

- Pitx2, Vglut2, parvalbumin in STN and Tac1 in *para*-STN are highly conserved mouse to primate
- Optogenetic excitation of STN or STN terminals in ventral pallidum causes aversive learning
- Optogenetic excitation of associated *para*-STN generates a distinctly different response
- Anatomical-functional dissection of STN vs. *para*-STN provides framework for emotional affect

Authors

Gian Pietro Serra, Adriane Guillaumin, Bianca Vlcek, ..., Jérôme Baufreton, François Georges, Åsa Wallén-Mackenzie

Correspondence

asa.mackenzie@ebc.uu.se

In brief

Serra et al. identify aversive learning and avoidance, sufficiently potent to interrupt positive reinforcement behavior, as direct consequences of optogenetic excitation of the subthalamic nucleus (STN) or STN terminals in pallidum. Demonstration of direct causality on emotional affect advances knowledge of brain pathology involving aberrant STN activity, including Parkinson's disease.

Serra et al., 2023, Cell Reports *42*, 113328
November 28, 2023
https://doi.org/10.1016/j.celrep.2023.113328

CellPress

Cell Reports

CellPress
OPEN ACCESS

Article

A role for the subthalamic nucleus in aversive learning

Gian Pietro Serra,[1] Adriane Guillaumin,[1,2] Bianca Vlcek,[1] Lorena Delgado-Zabalza,[2] Alessia Ricci,[1] Eleonora Rubino,[1] Sylvie Dumas,[3] Jérôme Baufreton,[2] François Georges,[2] and Åsa Wallén-Mackenzie[1,4,*]

[1]Uppsala University, Department of Organism Biology, 752 36 Uppsala, Sweden
[2]University of Bordeaux, CNRS, IMN, UMR 5293, 33000 Bordeaux, France
[3]Oramacell, Paris, France
[4]Lead contact
*Correspondence: asa.mackenzie@ebc.uu.se
https://doi.org/10.1016/j.celrep.2023.113328

SUMMARY

The subthalamic nucleus (STN) is critical for behavioral control; its dysregulation consequently correlated with neurological and neuropsychiatric disorders, including Parkinson's disease. Deep brain stimulation (DBS) targeting the STN successfully alleviates parkinsonian motor symptoms. However, low mood and depression are affective side effects. STN is adjoined with *para*-STN, associated with appetitive and aversive behavior. DBS aimed at STN might unintentionally modulate *para*-STN, causing aversion. Alternatively, the STN mediates aversion. To investigate causality between STN and aversion, affective behavior is addressed using optogenetics in mice. Selective promoters allow dissociation of STN (e.g., *Pitx2*) vs. *para*-STN (*Tac1*). Acute photostimulation results in aversion via both STN and *para*-STN. However, only STN stimulation-paired cues cause conditioned avoidance and only STN stimulation interrupts on-going sugar self-administration. Electrophysiological recordings identify post-synaptic responses in pallidal neurons, and selective photostimulation of STN terminals in the ventral pallidum replicates STN-induced aversion. Identifying STN as a source of aversive learning contributes neurobiological underpinnings to emotional affect.

INTRODUCTION

By executing major influence over motor, cognitive, and limbic function, the subthalamic nucleus (STN) is a critical component of the elaborate brain network governing behavioral control and flexibility.[1–16] Consequently, aberrant STN firing contributes to vastly complex dysfunction, as observed in, e.g., Parkinson's disease (PD), characterized by a range of motor and non-motor (affective, cognitive, physiological) symptoms[1,4,17] and obsessive-compulsive disorder (OCD), signified by obsessive thoughts and/or compulsive behavior.[18] Degeneration of STN neurons is a hallmark of supranuclear palsy and Huntington's disease,[19–21] further pinpointing the importance of STN in behavioral regulation. Deep brain stimulation (DBS) aiming to correct aberrant STN firing activity shows high success rate in symptom-alleviation in advanced-stage PD and treatment-resistant OCD, and is today a prioritized treatment.[18,22] STN-DBS has been forwarded as treatment for additional disorders[23] such as refractory Tourette's syndrome,[24,25] while recent research on the STN in reward-related behavior has highlighted STN-DBS as a promising intervention candidate for substance use disorder.[26–31] Already an important treatment method, and with increasing interest propelled toward additional implementation in patients, one major challenge with STN-DBS that remains to be solved is the emergence of adverse side effects. Some STN-DBS-induced side effects resemble psychiatric disorder, including apathy and depression.[23,32] Adverse side effects draw attention to the urgency of unraveling the plethora of roles played by the STN, not least in affective function.

Adding to the complexity of the STN is its small size and its position in a functionally diverse brain area at the thalamic-hypothalamic-midbrain intersection. Surrounded by passing fibers that traverse vastly within the brain,[33–37] the STN is adjacent to the zona incerta (ZI), a DBS-target in PD, co-morbid PD/OCD, and tremor,[36,38,39] and directly fused with *para*-STN (pSTN), associated with feeding behavior, novelty response, and recently implicated in aversion.[37,40–46] Treatment strategies aiming to probe dysregulated STN neurons by intra-cranial insertion of electrical leads thereby stands at risk of affecting functionally diverse neurons within the STN as well as neighboring structures that subserve regulation over other types of behaviors than those intended for treatment, and that instead may be the direct cause of adverse side effects. To advance precision in treatment and reach symptom alleviation without causing unwanted side effects, experimental strategies in rodents that enable dissociation, and hence revelation, of the full repertoire of behaviors mediated by the subthalamic area are necessary.

The STN receives excitatory regulation from the cerebral cortex and inhibitory regulation from the basal ganglia.[1,47] Mimicking excitatory and inhibitory stimulation of the STN in an optogenetic paradigm in mice, we and others recently described how STN excitation induced flighting behavior and stereotypic grooming.[48,49] These findings challenge the current

roles ascribed to the STN by opening up for the possibility that STN mediates aversive behavior. Further supported by reports of aberrant STN activity in PD and negative affect, such as non-motor symptoms in PD and adverse side effects upon STN-DBS, we hypothesized that the STN exerts influence on behavioral aversion, and that such STN-driven aversion is distinct from pSTN-driven affect.

To address causality between STN and aversion, and to functionally tease out the STN from pSTN, this study took advantage of promoters that allow spatial dissociation of these anatomically associated structures. A translational comparison between mouse and macaque monkey was performed, followed through with optogenetics-driven neurocircuitry and behavior analysis in mice with focus emotional affect.

RESULTS

Anatomically associated STN and pSTN are distinguishable by molecular markers

The STN is located between the cerebral peduncle and ZI, and joined medially to the pSTN (Figure 1A). Fluorescent *in situ* hybridization (FISH) verified previous data that the majority of STN neurons in the mouse are positive for vesicular glutamate transporter 2 (*Vglut2*) (Figures 1B, 1D, and 1F)[48,50–52] and paired-like homeodomain 2 (*Pitx2*) (Figures 1C, 1E, and 1F)[52–54] mRNAs. *Vglut2* is abundant in surrounding thalamus and hypothalamus (Figures 1B and 1D), whereas *Pitx2* is almost entirely selective for STN, with rare distribution outside (Figures 1C and 1E). *Vglut2* and *Pitx2* labelings are denser in medial than lateral STN (Figures 1D [D1 vs. D2] and 1E [E1 vs. E2]), but overlap completely (Figures 1F1 vs. F2), and $STN^{Pitx2/Vglut2}$ double-labeling covers the entire STN (Figures 1D–1F). Parvalbumin (*PV*) has been described as an STN marker.[55–59] In accordance with literature, *PV* mRNA is stronger in dorsal than medial STN (Figure 1G [G1 vs. G2]); however, scattered PV^+ cells are present throughout the STN, forming a subpopulation (STN^{PV}) (Figures 1G–1I2). Dorsal to STN, *PV* is abundant in ZI (Figure 1G).

In our previous implementation of single-nuclei RNA sequencing, transcriptional products were identified in the STN and surrounding structures.[58] This approach identified tachykinin precursor 1 (*Tac1*) mRNA as a marker for pSTN ($pSTN^{Tac1}$). Here, high selectivity of *Tac1* mRNA in pSTN was detected (Figure 1J), with very few, if any, $Tac1^+$ cells in the STN (Figures 1J–1L); *Tac1* and *Pitx2* thus forming a distinct border between pSTN ($Tac1^+$) and STN ($Pitx2^+$), adjoined at the medial STN (Figures 1J1–L1). Having confirmed *Tac1* in pSTN and *Pitx2* in STN, two primarily excitatory structures, it was of interest to assess any presence of inhibitory neurons; for this, glutamic acid decarboxylase (*Gad1*) mRNA was analyzed, which confirmed the GABAergic identity of the ZI, and the presence of only very rare $Gad1^+$ neurons in STN and pSTN (Figures 1M–1O).

Here, we showed that ZI and STN readily can be distinguished as two cellular densities, while pSTN is more difficult to dissociate from STN (Figure 1P). However, by comparison of distribution patterns for selected molecular markers, STN (*Pitx2*) and pSTN (*Tac1*) can be detected as distinctly separate structures: medial STN dissociated from pSTN (Figure 1O).

Markers dissociating STN vs. pSTN show high translation toward primates

Next, the level of translation between rodent and primate STN and pSTN was assessed. For this, FISH co-labeling of serial sections using two probes per analysis (Vglut2/Pitx2; Tac1/Vglut2; Tac1/Pitx2; PV/Tac1; PV/Pitx2; Vglut2/Gad1) was qualitatively and quantitatively analyzed in the mouse (Figures 2A1–F4 and M1–N4) and macaque monkey (Figures 2G1–J1 and O1–O4), and results between the species compared (Figures 2K and 2P). The results identified a striking similarity between mouse and macaque *Pitx2*, *Vglut2*, *PV*, and *Tac1* mRNAs, both in terms of spatial distribution of the markers and their respective overlap. By visual inspection, all four markers were confirmed in similar distribution patterns for macaques as described above for mice. Furthermore, by careful assessment at the STN and pSTN intersection (Figures 2A2–F4, mouse, and 2G2–H4′, macaque), the opposite patterns of *Vglut2* and *Pitx2* (STN) vs. *Tac1* (pSTN) confirm a distinct border between STN and pSTN in both species. Rare $Pitx2^+$ cells are present in pSTN, found close to this border; *Vglut2* is more common than *Pitx2* in pSTN, but still far less of both than in STN. In the macaque, *Tac1* shows similar distribution pattern as in the mouse, with far more in pSTN than STN; however, its detection is overall weaker in macaques. Rare GABA cells could be identified in pSTN of both mouse and macaque using Gad1 and Gad2 (Figures 2M–2O).

Quantification (Figure 2K) demonstrates 100% co-labeling *Vglut2*/*Pitx2* in STN of both species, and the majority of STN is $Vglut2^+$/$Pitx2^+$; far less $Vglut2^+$/$Pitx2^+$ in pSTN (of $Vglut2^+$ cells, 35% vs. 56% $Pitx2^+$ in mouse vs. monkey); *Tac1* is highly selective for pSTN in both species, and a proportion of $Tac1^+$ cells is positive for *Vglut2* (pSTN: $Tac1^+$/$Vglut2^+$ 72% mouse vs. 42% monkey; STN: less than 2% $Tac1^+$). The analysis also revealed the presence of $Vglut2^+$ pSTN neurons negative for *Tac1*; $Vglut2^+$/$Tac1^-$, twice more common in macaque (55%) than mouse (24%), validating the visual inspection. No PV^+ cells were identified in pSTN of either species; however, in STN, the intensity of *PV* labeling could be further subgrouped into "high" and "low" with PV^{high} cells toward the lateral STN of macaques (Figures 2J1–J4); the quantification identifying PV^{high}/*Vglut2* and PV^{low}/*Vglut2* STN cells in a similar percentage in both species, and also identification of PV^+ cells negative for *Vglut2*. A schematic summary allows visualization of significant spatio-molecular translation in STN and pSTN between mouse and macaque (Figure 2P).

Almost mutually exclusive targets for STN (motor, limbic) and pSTN (limbic)

To address the hypothesis that STN mediates aversion, an optogenetic behavior and neurocircuitry analysis was next performed, taking advantage of the spatial selectivity offered by the promoters in mice, and validated in primates, for STN (*Pitx2*, *Vglut2*, *PV* [STN-subpopulation]) and pSTN (*Tac1*). Corresponding Cre-recombinase mouse lines (Pitx2-Cre, Vglut2-Cre, PV-Cre, and Tac1-Cre) were injected with adeno-associated virus 2 (AAV2) carrying a construct encoding either channelrhodopsin-2 (ChR2) fused with reporter (enhanced yellow fluorescent protein [eYFP]), or, as controls, a similar construct with only reporter (eYFP). Experimental

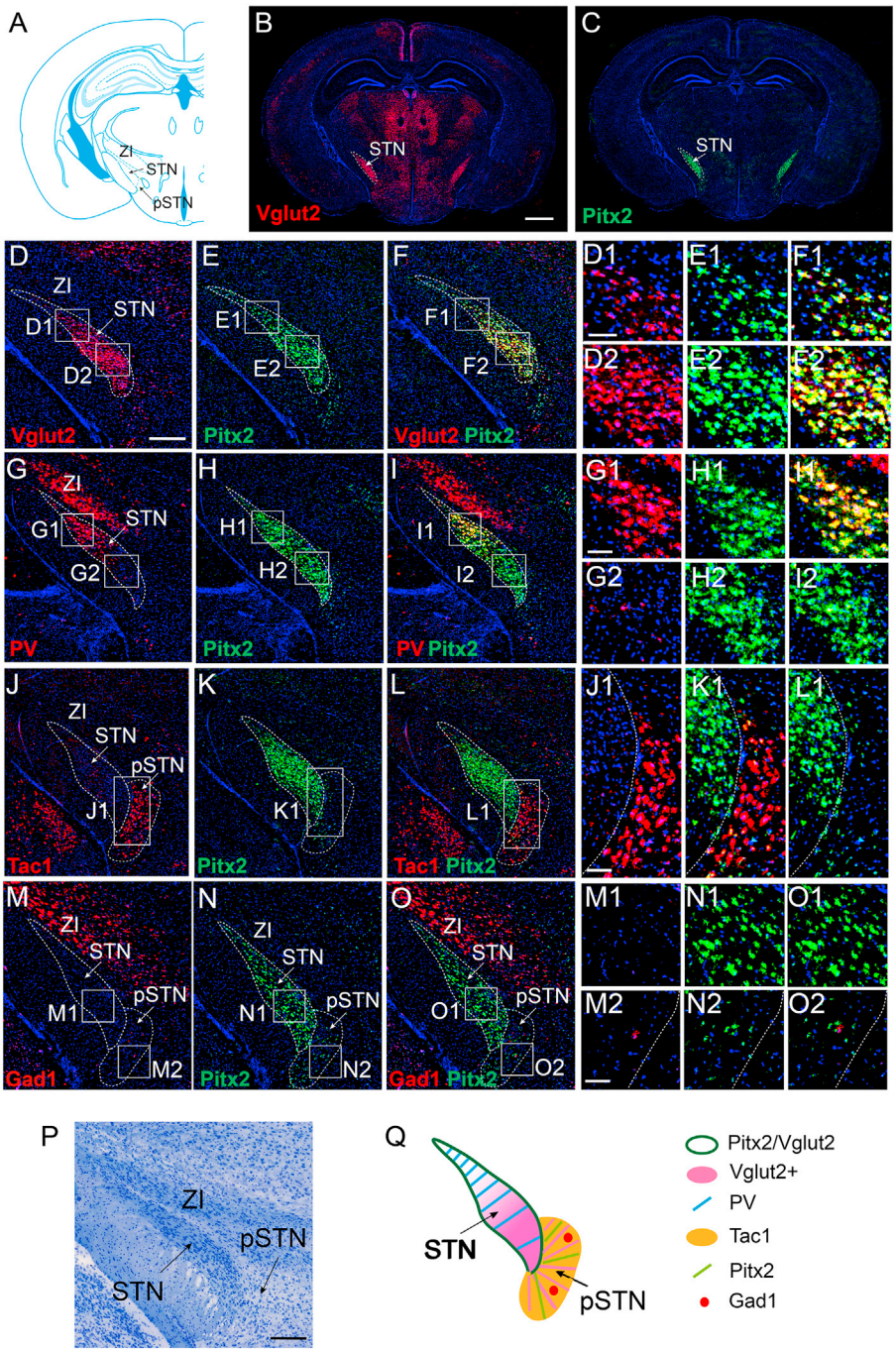

Figure 1. Anatomically associated STN and pSTN distinguishable by molecular markers

(A) Coronal mouse brain sections. Schematic illustration: subthalamic nucleus (STN), *para*-subthalamic nucleus (pSTN), and zona incerta (ZI); bregma −2.18.[60]

(B–O) Fluorescent *in situ* hybridization (FISH) of STN/pSTN/ZI area; mRNA at same bregma. (B and C) Overviews, *Vglut2* (B), *Pitx2* (C). (D–O2) Single fluorescent channel. (D–N) single mRNA labeling. Dual channels (both mRNAs) (F–O). Corresponding cellular close-ups within squares displayed in main panels: *Vglut2* (D-D2), *Pitx2* (E-E2), (*Vglut2*/*Pitx2*) (F-F2), *PV* (G-G2), *Pitx2* (H-H2), *PV*/*Pitx2* (I-I2), *Tac1* (J-J1), *Pitx2* (K-K21), *Tac1*/*Pitx2* (L-L1), *Gad1* (M-M2), *Pitx2* (N-N2), and *Gad1*/*Pitx2* (O-O2).

(P) Cresyl violet; same bregma.

(Q) Schematic summary. Serial sections analyzed for each probe pair (co-labeling with Pitx2). mRNA (number of brains): *Vglut2* (n = 8), *PV* (n = 5), and *Tac1* (n = 4). Scale bars, 1 mm (B), 300 μm (D), 70 μm (D1, G1, and M2), 300 μm (P). Full mRNA names in main text.

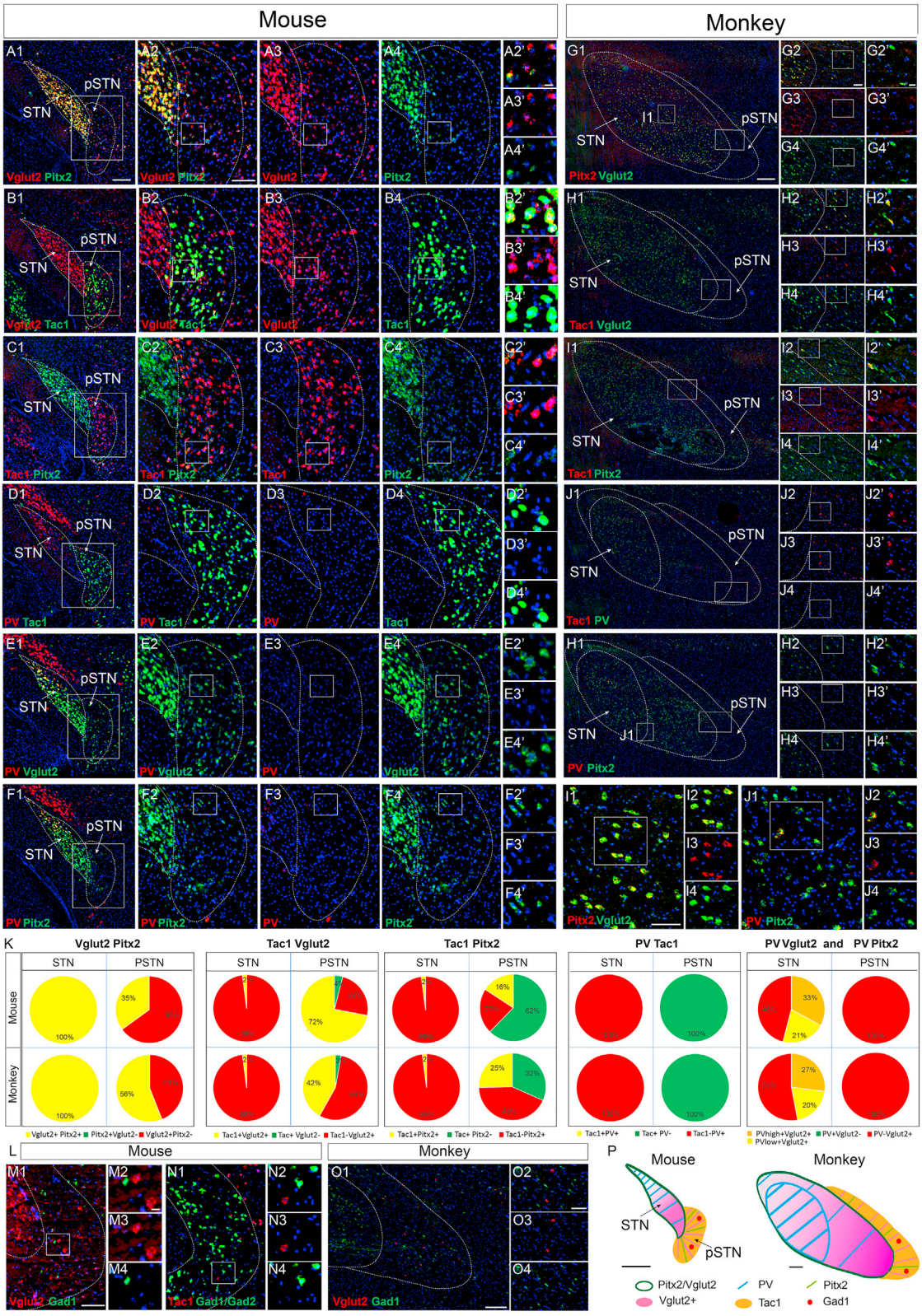

(legend on next page)

groups (Pitx2/ChR2, Vglut2/ChR2, PV/ChR2, and Tac1/ChR2) and control groups (Pitx2/CTRL, Vglut2/CTRL, PV/CTRL, and Tac1/CTRL) taken together; mouse groups summarized as STN^{Pitx2}, STN^{Vglut2}, STN^{PV}, and $pSTN^{Tac1}$.

First, the validity of each injected Cre-driver was confirmed by YFP-immunofluorescent reporter analysis. At the level of the injection site, distinct cellular labeling was observed in STN for injected STN^{Pitx2}, STN^{Vglut2}, and STN^{PV} mice (Figures 3B_0–D_0 and S1), and in pSTN for injected $pSTN^{Tac1}$ mice (Figures 3E_0 and S1). In STN^{Vglut2} mice, scattered YFP-positive cells were detected in pSTN, in accordance with mRNA analysis (above). Analysis of YFP labeling in projections allowed the confirmation of projections from STN^{Pitx2} neurons in pallidal structures: entopeduncular nucleus (EP) (globus pallidus [GP] interna in primates), GP (GP externa in primates), ventral pallidum (VP), and also nigral structures of midbrain (substantia nigra pars reticulata [SNr] and pars compacta [SNc]) (Figures 3$B_{1–7}$), thus reaching both motor and limbic areas in accordance with our recent report of STN^{Pitx2} mice.[48] No YFP was detected in lateral habenula, LHb. STN^{Vglut2} and STN^{PV} neurons showed similar, but not identical, projections (Figures 3$C_{1–7}$ and $D_{1–7}$). STN^{Pitx2} and STN^{PV} projections were strongest in EP, GP, and SNr (Figures 3$B_{4,5,7}$ and $C_{4,5,7}$). YFP analysis of injected $pSTN^{Tac1}$ mice identified projections to limbic structures, including central amygdala, septum, and bed nucleus of the stria terminalis (Figures 3$E_{1–7}$), in accordance with a recent report.[42] In addition, $pSTN^{Tac1}$ projections were identified in SNc and VP (Figures 3E_2 and E_7). STN^{Vglut2} showed projections to some of the same structures (Figure 3C_{1-7}), whereas STN^{PV} showed no YFP labeling in these areas and STN^{Pitx2} projections were either weak or absent. $pSTN^{Tac1}$ projections to EP, GP, and SNr were sparse or nonexistent (Figure 3E_{1-7}). Thus, STN^{Pitx2} and $pSTN^{Tac1}$ target areas were almost mutually exclusive, apart from SNc and VP, which received projections from both STN and pSTN.

Optogenetic stimulation of either STN or pSTN induces repetitive grooming

Next, behavioral assessment was initiated, for which injected mice of all four lines were implanted with fiber optic probes, and their response to photostimulation in a battery of tests relevant to aversive behavior was tested. Post-experiments, brains were analyzed for YFP distribution and placement of probes (Figures S1 and S2).

Based on recent reports of grooming and jumping behavior upon optogenetic STN excitation,[48,49] mice were first analyzed in an open-field apparatus coupled with laser activation (Opto-Open Field) (Figure S3). Grooming follows a cephalo-caudal rule and is a normal cleansing behavior for rodents.[61,62] However, when accentuated, self-grooming has been correlated with anxiety and/or aversion.[63,64] Behavior during periods of photostimulation (Light-ON) was compared with periods of no photostimulation (Light-OFF). Pitx2/ChR2, Vglut2/ChR2, and Tac1/ChR2 mice all responded to stimulation with repetitive face grooming (Figure S3). PV/ChR2 mice did not respond to photostimulation at all, instead this group of mice was similar to all control groups (Figure S3). Pitx2/ChR2 and Tac1/ChR2 mice showed slight differences in response curves (frequency and latency) but the grooming was similar in appearance, whereas Vglut2/ChR2 mice responded with grooming and excessive jumping, precluding further analysis (Figure S3). Summarizing, STN and pSTN excitations both induce stereotypic face grooming, a possible indicator of aversion or anxiety.

Optogenetic excitation of STN but not pSTN induces aversive learning

Taking this result into consideration, the elevated plus maze (EPM) test was re-designed so that avoidance upon optogenetic stimulation is tested and compared with natural aversion. This is referred to as the Opto-Avoidance-EPM test. Here, entry into the closed, sheltered arms of the EPM apparatus was paired with photostimulation (Light-ON), while the open arms and center area remained unpaired (Light-OFF) (Figure 4F). This way, Opto-Avoidance-EPM allows direct comparison between a naturally aversive context (open arm) and aversion caused by induced subthalamic activation (photostimulation; closed arm). Applying this protocol, as expected, none of the control groups showed any effect of photostimulation; they preferred the sheltered, closed arms (Figures 4G–4J and S4). However, STN mice (Pitx2/ChR2; Vglut2/ChR2) (Figures 4G, 4H, and S4) and pSTN mice (Tac1/ChR2) (Figures 4J and S4) all actively avoided the photostimulation-paired arms, demonstrating aversive response. PV/ChR2 mice showed small but significant decrease in time spent in the photostimulation-paired arms (Figure 4I).

To further dissociate this observed behavior, aversion was further assessed using a modified version of the real time (RT) place preference test,[65,66] applied in a standardized conditioned place preference (CPP) apparatus. In the current protocol, referred to as Opto-RT-CPP, place avoidance in RT upon photostimulation was assessed, as well as the conditioned response upon presentation to photostimulation-associated cues. To further validate behavioral responses, the ability to reverse a learned response was assessed. The test was designed as follows: habituation (day 1); pre-test day (no light, day 2); two RT days, entry into compartment A (not B) paired with photostimulation (Light-ON A, days 3 and 4); two test days to assess conditioned response to photostimulation-paired cues (no light, days 5 and 6); two RT days, entry into compartment B (not A) paired with photostimulation (Light-ON B, days 7 and 8); one test day to assess the cue-induced response (no light, day 9) (Figure 4K).

As expected, none of the control groups showed photostimulation-related avoidance (Figures 4L–4O). In contrast, STN mice (Pitx2/ChR2, Vglut2/ChR2) actively avoided either compartment (A or B) that was paired with photostimulation. All STN mice spent

Figure 2. Markers dissociating STN vs. pSTN show high translation toward primates

Comparative analysis of subthalamic and *para*-subthalamic nuclei (STN and pSTN) in mouse and macaque monkey brains. Fluorescent *in situ* hybridization (FISH) in mouse (A1–F4) and macaque (G1–J4): *Pitx2* and *Vglut2* (A and G); *Tac1* and *Vglut2* (B and H); *Pitx2* and *Tac1* (C and I); *PV* and *Tac1* (D and J); *PV*, *Pitx2*, and *Vglut2* (E–J) mRNAs. Overviews, both mRNAs in panel 1, close-ups of border area, medial STN vs. pSTN in panels 2–4, both mRNAs, panel 2, single mRNA, panels 3 and 4. (K) Quantitative analysis: top panel, mouse; bottom panel, macaque monkey. FISH mouse (M and N), monkey (O): *Gad1*, *Gad2*, and *Vglut2* mRNAs. (P) Schematic summary. Serial sections analyzed for each probe pair. Full mRNA names in main text. Scale bars, as indicated.

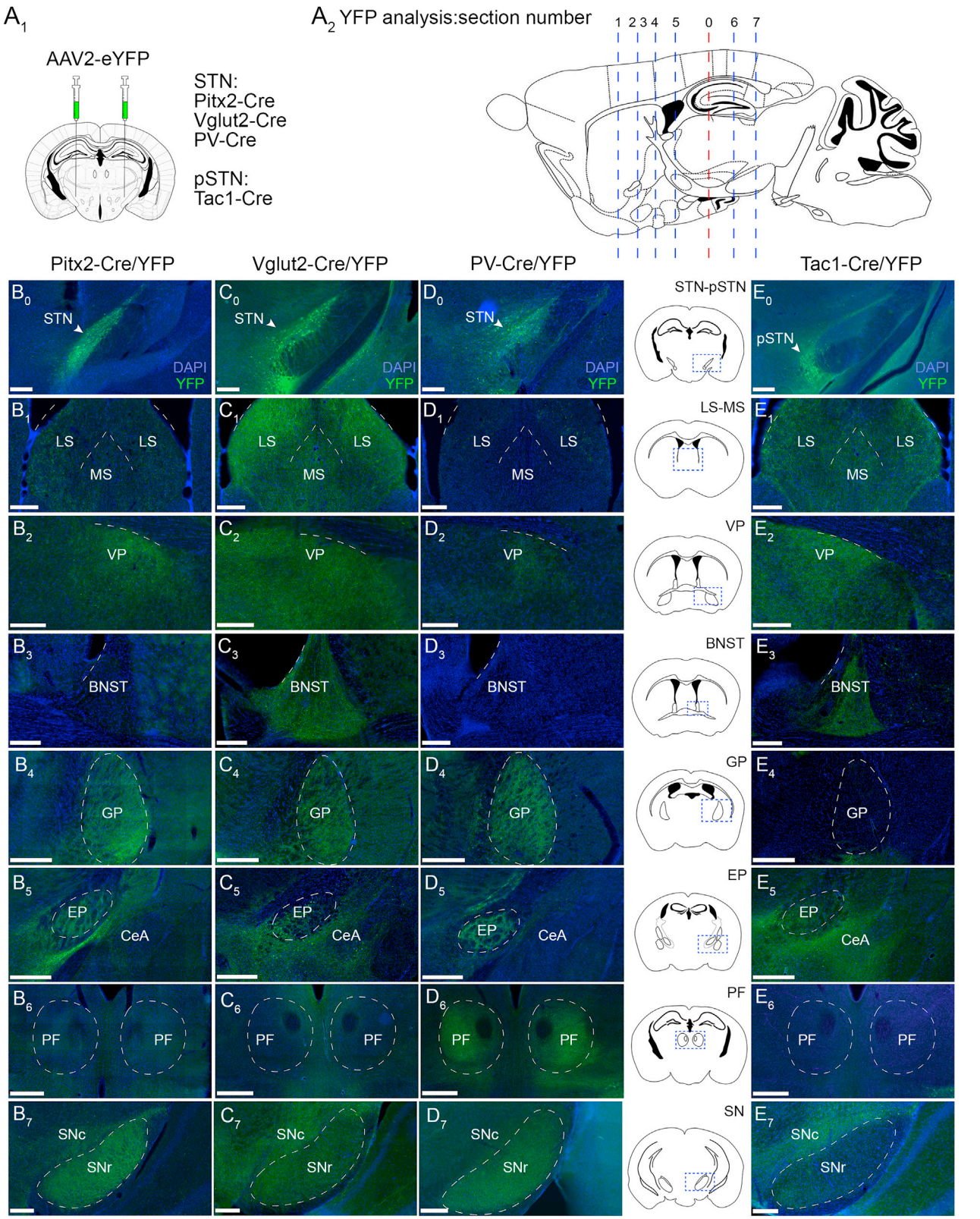

(legend on next page)

significantly less time in the photostimulation-paired compartment than the unpaired compartment when assessed in RT (Figures 4L′ and 4M′). Pitx2/ChR2 mice reduced the number of entries to the photostimulation-paired compartment (Figure S4). Furthermore, all STN mice demonstrated conditioned avoidance on test days, demonstrating a learned response. Pitx2/ChR2, but not Vglut2/ChR2, mice reached statistical significance (Figures 4L′, 4M′, and S4). All STN mice showed reversal response, but did not reach significant during test days.

Next, PV/ChR2 mice were analyzed and showed a similar response as Pitx2/ChR2 mice both during RT stimulation and test days, but did not show reversal (Figures 4N′ and S4).

Finally, when assessing how mice behaved upon pSTN stimulation, a different type of behavior was observed (Figures 4O′ and S4). Time spent in photostimulation-paired chamber at RT (days 3 and 4) was significantly less than in the unpaired compartment for Tac1/ChR2 mice (Figure 4O′), as also observed above for STN mice. However, Tac1/ChR2 mice showed a trend, even if not significant, toward increasing (rather than decreasing) the number of entries (Figure S4). On test days, Tac1/ChR2 mice failed to show conditioned place avoidance and instead displayed conditioned preference (Figures 4O′ and S4). Similar to STN mice, pSTN mice showed reversal response, but did not reach significance on the reversal test day.

STN stimulation but not pSTN stimulation suppresses sugar positive reinforcement

Based on the above findings, we hypothesized that optogenetic stimulation causing aversive behavioral avoidance in STN-stimulated mice should be sufficient to induce a negative reinforcement behavior. To test this hypothesis, we next attempted to assess whether Pitx2/ChR2 mice could learn to make active nose-pokes (NPs) to terminate STN optogenetic activation. In this opto-negative reinforcement paradigm (Opto-NR), Pitx2/ChR2 mice failed to acquire an active NP response to terminate optogenetic stimulation and the experiment was aborted.

Instead, we decided to address the hypothesis that optogenetic STN stimulation should be sufficient to disrupt an on-going positive reinforcement (PR) behavioral task, using sugar as the reinforcer. We also hypothesized that STN and pSTN mice would respond differently, given their almost opposite responses in the Opto-RT-CPP test.

To test these hypotheses, an instrumental sugar PR paradigm (Sugar-PR) was implemented using operant boxes equipped with two NP apertures coupled to a reward dispenser with one active setup (NP leads to sugar delivery; active NP) and one inactive setup (no sugar delivery; inactive NP). The original schedule applied consisted of three phases (phase 1, training to NP for sugar reward in a fixed ratio [FR] paradigm; phase 2, NP to earn sucrose paired with photostimulation; phase 3, sugar reinstatement, photostimulation removed) (Figures 5A and S5).

In the absence of photostimulation (phase 1), all Pitx2/ChR2 (Figure 5D) and control (Figure 5C) mice showed a significantly higher number of active compared with inactive NPs, earning sugar reinforcers. This was the expected response, given the positively reinforcing properties of sugar. With the coupling to STN photostimulation (phase 2), control mice continued the same behavior. In contrast, Pitx2/ChR2 mice strongly reduced their NP activity on the active NP, a direct consequence of optogenetic STN activation. The difference between active and inactive NPs was no longer significant as the active NPs dropped with the onset of photostimulation. With subsequent removal of photostimulation (phase 3), Pitx2/ChR2 mice resumed nose poking (similar to phase 1), with the number of active NPs significantly higher than the inactive ones. No difference in the number of active NPs were observed between Pitx2/ChR2 and control mice during phases 1 and 3, while there was a significant decrease selectively for Pitx2/ChR2 mice in the photostimulation phase (Figure S6). Similar results were obtained with Vglut2/ChR2 mice (Figures 5E and S6). The results from both STN recombinase mouse lines confirmed the hypothesis that STN activation was sufficient to cause an interruption of on-going sugar self-administration.

When testing the PV/ChR2 mice, no effect of STN-photostimulation was observed. (Figures 5H and S6). To address this result further, the previous sugar reinstatement phase (phase 3) was changed for optogenetic stimulation only (instead of sugar only), administered as a consequence of the active NPs (Figures 5F–5H and S5). This led to an initial increase in the number of active NPs (seeking), likely due to the absence of the reinforcing stimulus (sugar), followed by a progressive decrease in number of active NPs (extinction). After this followed a phase 4, in which sugar was again available (Figures 5F–5H and S6). As expected, this restoration of sugar only caused the number of active NPs to again become significantly larger than the inactive ones. Thus, the mice responded to sugar but not to photostimulation; no difference was observed between PV/ChR2 and control mice in any of the four phases (Figure S6).

Finally, analysis of Tac1/ChR2 mice did not show any aversive response upon optogenetic stimulation but continued nose-poking for sugar even in the presence of photostimulation (Figures 5J, 5K, and S6). Furthermore, using a phase 3 in which active NPs were coupled with photostimulation alone (no sugar), no decrease in the number of active NPs was achieved, but instead the number of inactive NPs increased until reaching the same values as the active ones (Figures 5K and S6). To assess this response further, two subsequent phases were added. Now, pSTN-photostimulation and sugar delivery were removed, leaving the acoustic cue as consequence of the active NPs (phase 4), and subsequently

Figure 3. Almost mutually exclusive targets for STN (motor, limbic) and pSTN (limbic)

Efferent projection analysis. (A) Experimental setup. Pitx2-Cre, Vglut2-Cre, PV-Cre, Tac1-Cre mice injected with AAV2-eYFP into STN/pSTN (A1). Illustration of mouse brain: dotted lines indicate section levels (0–7) displayed as coronal sections analyzed by YFP immunohistofluorescence below (note, level 0 shows injection site STN/pSTN) (A2).

(B–E) Selected sections from each injected mouse line and number of mice analyzed: B_{0-7}, Pitx2-Cre, n = 29; C_{0-7}, Vglut2-Cre, n = 29; D_{0-7}, PV-Cre, n = 18; E_{0-7}, Tac1-Cre, n = 18. Panel between (D and E): illustrations of areas shown per section level (squares). STN, subthalamic nucleus; pSTN, *para*-subthalamic nucleus; VP, ventral pallidum; GP, globus pallidus; EP, entopeduncular nucleus; CeA, central amygdala; BNST, bed nucleus of stria terminalis; PF, parafascicular thalamic nucleus; SNr, substantia nigra pars reticulata; SNc, substantia nigra pars compacta; LS, lateral septum; MS, medial septum.

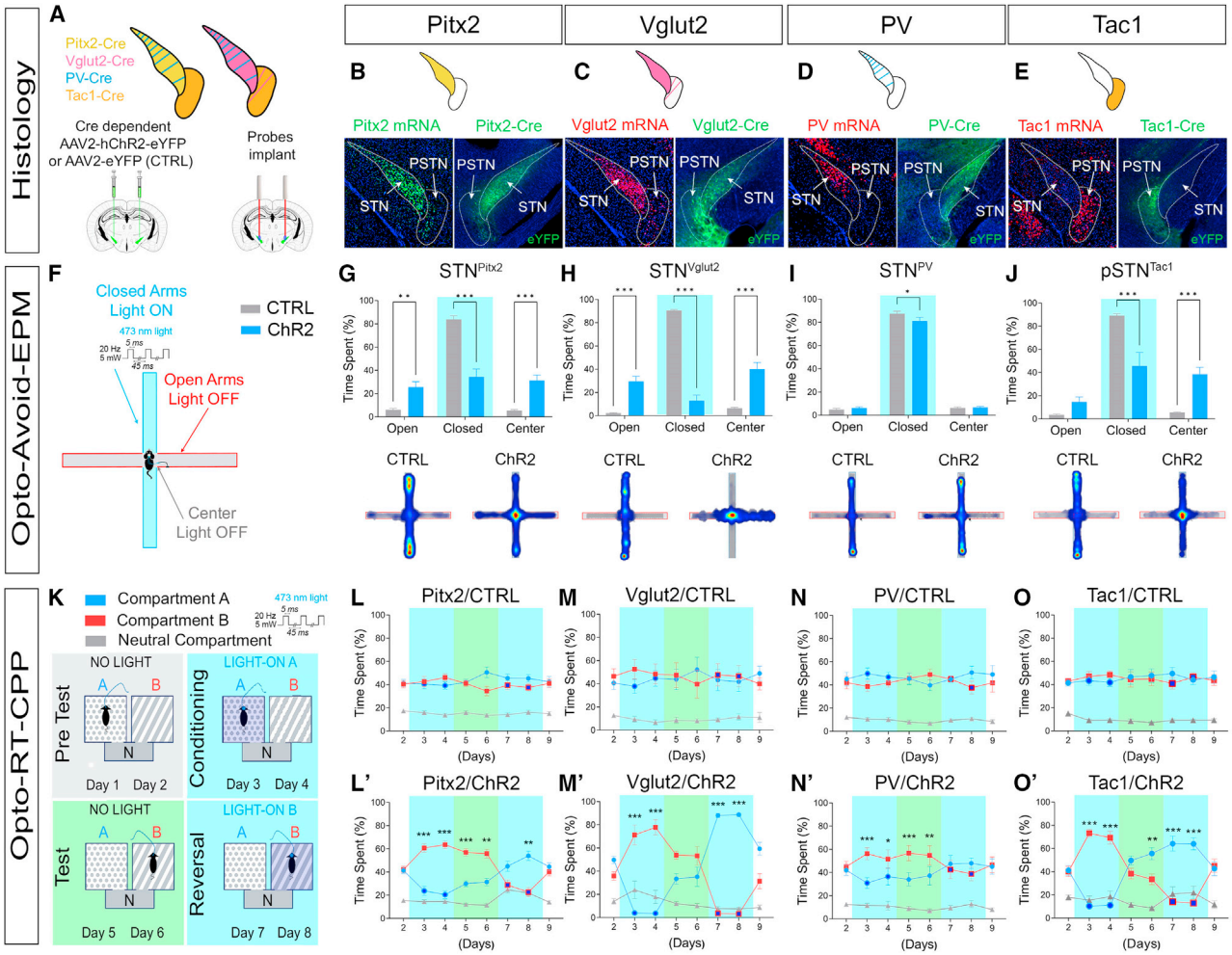

Figure 4. Optogenetic excitation of STN but not pSTN induces aversive learning

Battery of behavioral tests relevant for emotional affect.

(A) Illustration: STN, pSTN; color-coded for markers, simplified adaptation from Figure 1 (top). Bilateral AAV injection (AAV2-hChR2-eYFP [ChR2] or AAV2-eYFP [control; CTRL]) and fiber optic probe implantation above the subthalamus in Pitx2-Cre, Vglut2-Cre, PV-Cre, and Tac1-Cre mice (bottom).

(B–E) STN, pSTN histology. Left, mRNA; right, corresponding YFP of each injected Cre-recombinase mouse line: Pitx2/Pitx2-Cre (B), Vglut2/Vglut2-Cre (C), PV/PV-Cre (D), and Tac1/Tac1-Cre (E).

(F–J) Opto-avoidance EPM test. Graphical illustration of setup (F), time spent in arms (G–J). CTRL vs. ChR2; below, heatmaps. Pitx2/ChR2 (n = 16), Pitx2/CTRL (n = 15) (G); Vglut2/ChR2 (n = 7), Vglut2/CTRL (n = 5) (H); PV/ChR2 (n = 10), PV/CTRL (n = 9) (I); Tac1/ChR2 (n = 11), Tac1/CTRL (n = 10) (J) mice.

(K–S) Opto-RT-CPP test. Graphical illustration of setup. Blue, compartment A; red, compartment B; gray, neutral compartment (K). Percentage of time spent. Compartment A vs. compartment B: Pitx2/CTRL (n = 14) (L); Vglut2/CTRL (n = 5) (M); PV/CTRL (n = 9) (N); Tac1/CTRL (n = 10) (O); Pitx2/ChR2 (n = 16) (L′), Vglut2/ChR2 (n = 7) (M′), PV/ChR2 (n = 10) (N′), and Tac1/ChR2 (n = 10) (O′). Dark blue filled circles (compartment A) and squares (compartment B) indicate photostimulation (Light-ON). Data were analyzed by two-way RM ANOVA (G–J and L–O′) followed by Šídák's multiple comparisons test (G–J) or Tukey's multiple comparisons test (L–O′). *p < 0.05, **p < 0.01, ***p < 0.001. Data expressed as mean ± SEM. n, number of mice. STN, subthalamic nucleus; pSTN, *para*-subthalamic nucleus.

removing also the cue, so that active NPs were equal to inactive NPs (phase 5) (Figures 5I and S5). Tac1/ChR2 mice responded during the first sessions of phase 4 with strongly increased number of active NPs (seeking) and then proceeded toward extinction during the following sessions (Figure 5K). This result was different to that observed with controls as these showed a strong increase in active NPs when sugar was removed (Figure 5J).

In contrast to STN stimulation, which interrupted self-administration, activation of the pSTN did not negatively affect sugar consumption, instead pSTN mice maintained their self-administration activity.

Optogenetic stimulation of STN is sufficient to induce excitatory post-synaptic responses in LHb

Since excitation of the STN but not the pSTN promoted strong aversion learning leading to contextual avoidance behavior, exploring a putative STN neurocircuitry of aversion was next of interest.

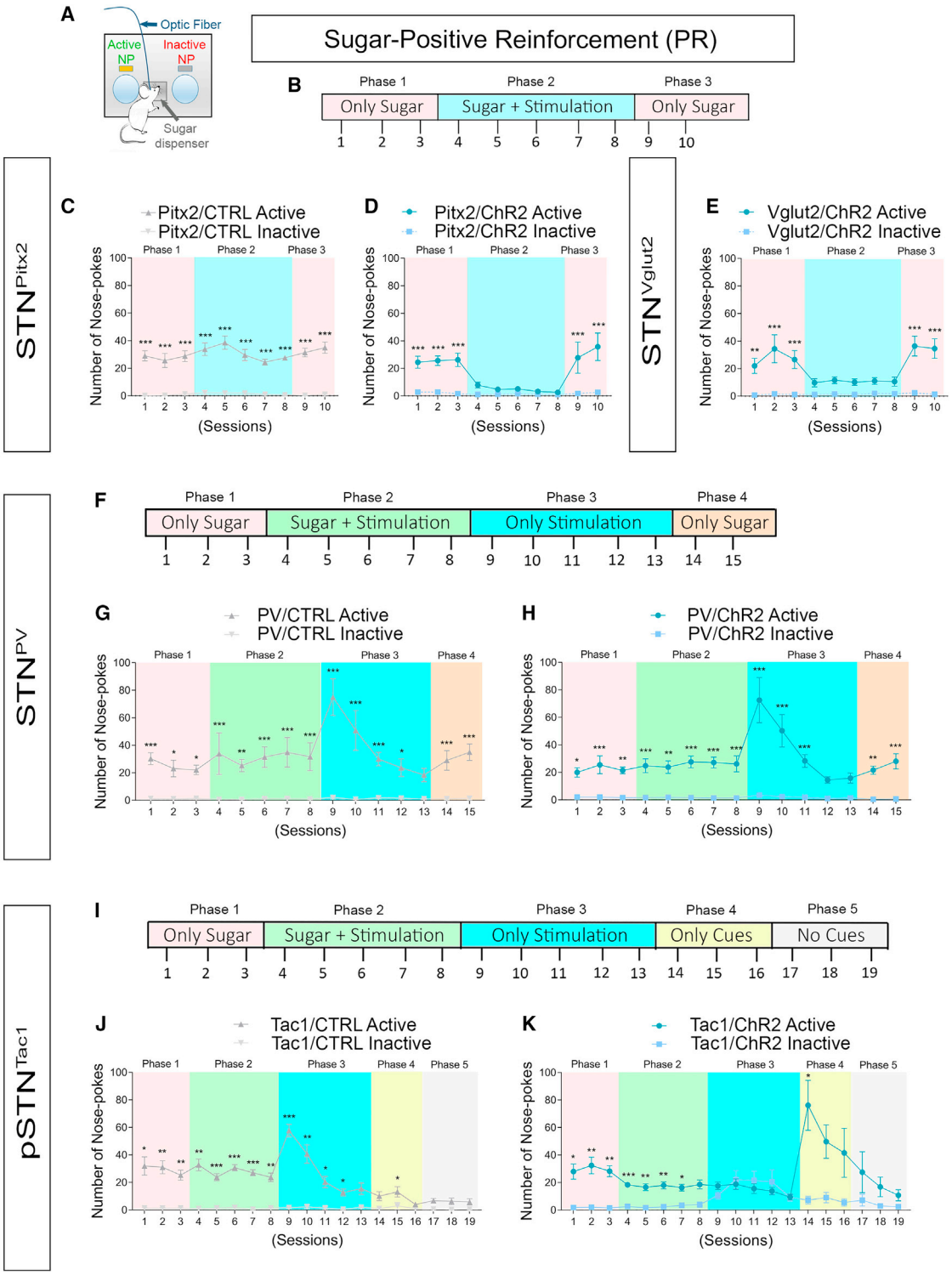

Figure 5. STN stimulation but not pSTN stimulation suppresses sugar-positive reinforcement

Sugar self-administration combined with optogenetic STN or pSTN excitation; positive reinforcement (PR) test. Graphical illustration of setup (A) and original protocol (B). (C–K) (Pitx2: C and D; Vglut2: E; PV: F–H; Tac1: I-K) Number of active vs. inactive nose-pokes: Pitx2/CTRL (n = 5) (C), Pitx2/ChR2 (n = 8) (D), Vglut2/ChR2 (n = 5) (E), PV/CTRL (n = 7) (G) PV/ChR2 (n = 10) (H), Tac1/CTRL (n = 9) (J), and Tac1/ChR2 (n = 11) (K). Modified protocol displayed in (F) and (I). Data were analyzed by two-way RM ANOVA followed by Šídák's multiple comparisons test. Data expressed as mean ± SEM. *p < 0.05, **p < 0.01, ***p < 0.001. n, number of mice. STN, subthalamic nucleus; pSTN, *para*-subthalamic nucleus.

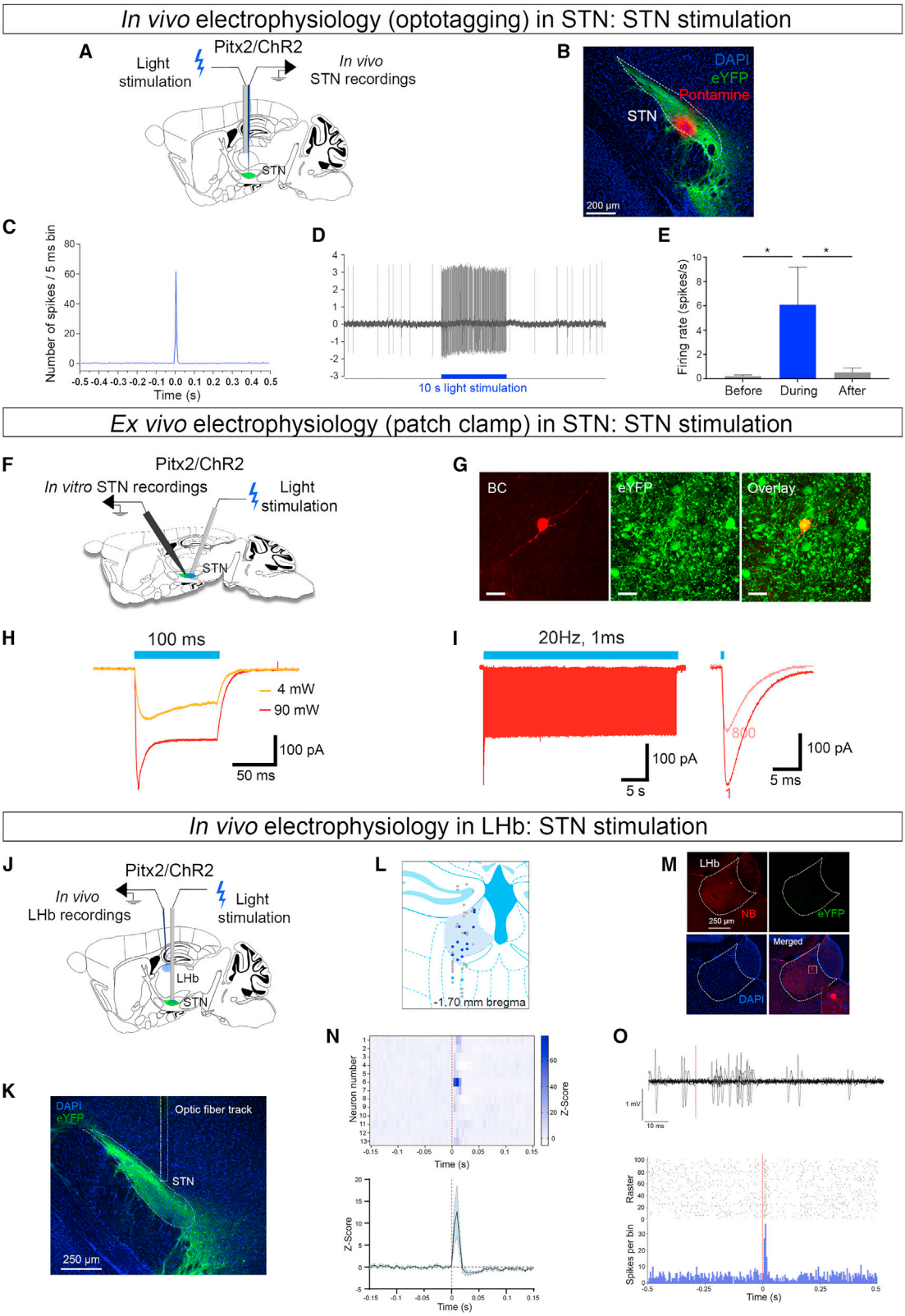

(legend on next page)

First, *in vivo* single-cell electrophysiological recordings upon optogenetic stimulation of the STN were performed in Pitx2/ChR2 mice to verify activational response of STN neurons (Figures 6A and 6B). An optotagging protocol (Figure 6A) was used to stimulate and record within the STN. To observe the reaction of STN neurons to photostimulation, peri-stimulus time histograms (0.5 Hz, 5 ms bin width, 5–8 mW) were created by applying a 0.5 Hz stimulation protocol for at least 100 s. Action potentials in ChR2-positive STN cells were successfully evoked by STN photostimulation (Figure 6C). Once neuronal activity of STN neurons returned to baseline, the photostimulation protocol used in the behavioral experiments was assessed (20 Hz, 5 ms pulses, 5–8 mW; 10 s), which increased the frequency and firing rate of STN neurons for the whole duration of the stimulation, after which they returned to normal (Figures 6D and 6E).

The functional expression of ChR2 on STN neurons was next confirmed by *ex vivo* patch-clamp recordings in the STN of Pitx2/ChR2 mice with the optic probe placed above the recording site (Figure 6F). YFP labeling was strong in the STN (Figure 6G), and all recorded STN neurons responded to continuous (Figure 6H) or 20 Hz trains (Figure 6I) of photostimulation by sustained ChR2-mediated currents. When photostimulation was applied in brain slices from Pitx2/CTRL control mice, no current was observed in STN neurons.

Having validated our optogenetic strategy, potential neurocircuitry was next addressed. STN-DBS has repeatedly been reported to give rise to depression as adverse side effect,[23,32] providing a clinical association between STN stimulation and negative emotional affect. Furthermore, STN-DBS in rodents induces c-Fos expression in LHb and alters LHb neuron activity,[67,68] suggestive of functional connectivity between STN and the LHb. However, projection analysis did not reveal YFP-positive projections in the LHb of STN^{Pitx2} mice (Figure 3 and electrophysiological controls; Figure 6M) while ample other projections were indeed observed (Figure 3).[48]

To explore if STN-activation exerts functional impact on LHb activity, *in vivo* extracellular recordings were performed in Pitx2/ChR2 mice (Figure 6J). An optic fiber was positioned above the STN and a stimulation protocol (PSTH: 0.5 Hz, 5 ms pulses, 5–8 mW, at least 100 s) was implemented (Figures 6J and 6K). Post-recording, pontamine staining and neurobiotin-marked neurons confirmed the positioning of the recording electrodes within the LHb (Figures 6L and 6M). Analysis showed that STN stimulation evoked an excitatory response in 50% of the recorded LHb neurons (onset latency = 10.08 ± 0.81 ms) (Figures 6N and 6O). Thus, a functional STN-LHb connection could be observed. With the observed lack of direct projections from STN to LHb (confirmed by the absence of eYFP fibers in LHb; Figure 6M), identification of a putative pathway was next approached.

Optogenetic activation of STN projections induces excitatory post-synaptic responses in VP and EP neurons projecting to LHb

Rather than direct projections from STN to LHb, STN^{Pitx2} mice showed abundant projections to pallidal structures VP and EP, as verified above (Figure 3) and reported previously.[48] Both VP and EP, in turn, have been shown to project to LHb.[69–72] Based on these observations, the STN-VP and STN-EP pathways were next examined, taking advantage of the Vglut2-positive nature of both STN and LHb.

Using rgAAV2-DIO-GFP injections in the LHb of Vglut2-Cre mice, Vglut2-expressing LHb-projecting VP and EP neurons were retrogradely labeled. An AAV5-DIO-CHR2-mCherry vector was injected in the STN of the same mice to selectively manipulate STN-VP and STN-EP pathways with photostimulation (Figures 7A and 7B). Two to 3 weeks later, acute brain slices were prepared and GFP-expressing VP and EP neurons were recorded in voltage-clamp configuration and filled with biocytin (Figures 7C–7F and 7I). STN inputs were optically stimulated and synaptic inputs were recorded in GFP-positive VP and EP neurons, respectively. One hundred percent of the recorded LHb-projecting EP neurons were identified as responsive to STN inputs stimulation, while only 50% of LHb-projecting VP display light-evoked synaptic currents (Figures 7G, 7H, 7J, and 7K). The amplitude of the excitatory postsynaptic currents (EPSCs) was significantly greater (Figure 7L) and the latency of the EPSC significantly shorter (Figure 7M) in EP neurons compared with VP neurons. These results suggest that two distinct di-synaptic pathways relay the STN to the LHb.

Figure 6. Optogenetic stimulation of STN is sufficient to induce excitatory post-synaptic responses in LHb

(A) *In vivo* STN optotagging strategy.
(B) Pontamine sky blue (red) shows last recorded coordinate of STN neurons (green).
(C) Averaged PSTH of STN-excited neurons.
(D) STN-excited neuron recording trace.
(E) Frequency of STN neurons before, during, and after 10 s stimulation (n = 7).
(F) Patch-clamp strategy: electrode and optic fiber placed above STN.
(G) ChR2-YFP-positive STN neuron (green) filled with biocytin (BC, red). Scale bar, 10 μm.
(H) Representative ChR2-mediated currents induced by 1 s light pulses at 4 mW (yellow) and 90 mW (red).
(I) ChR2-mediated currents induced by train (40 s duration; 20 Hz; 1 ms pulses) of light.
(J) *In vivo* LHb recording strategy upon STN photostimulation.
(K) YFP (green); optic fiber track above STN.
(L) Map of LHb recorded neurons (n = 44; 3 mice): LHb neurons excited during stimulation (dark blue), excited neurons outside LHb (light blue), and non-responding neurons (gray).
(M) Excited LHb neuron; neurobiotin.
(N) PSTH heatmap; excited LHb neurons upon STN-photostimulation (top); average of normalized PSTH (bottom; n = 13 neurons).
(O) LHb neuron responding to STN photostimulation: 5 ms light pulse (10 traces; top); PSTH; raster of excited LHb neuron (below). Data were analyzed by Friedman test followed by Dunn's multiple comparisons. Data expressed as mean ± SEM. *p < 0.05. n, number of neurons unless indicated. STN, subthalamic nucleus; LHb, lateral habenula.

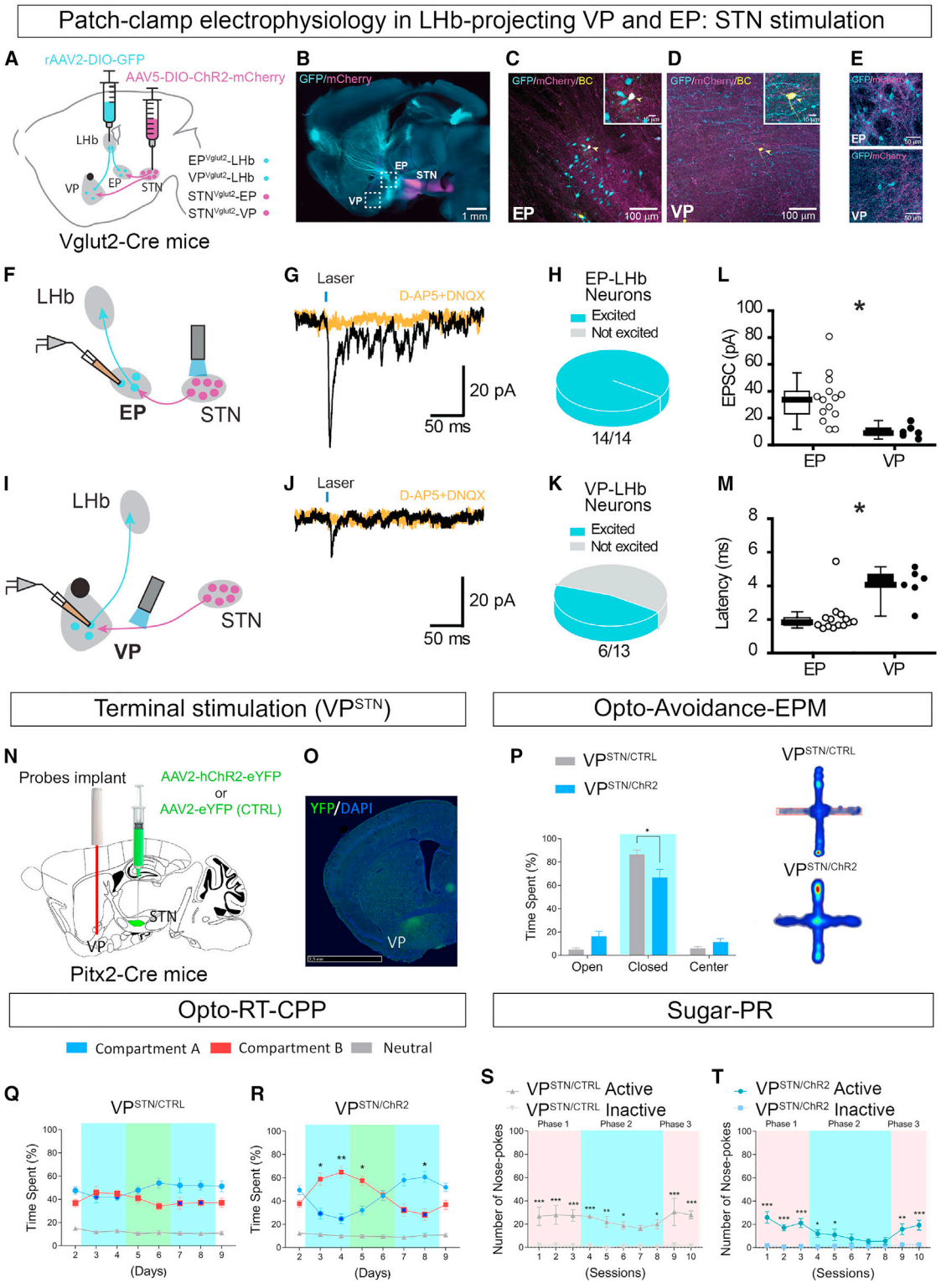

Figure 7. Optogenetic activation of STN projections induces excitatory post-synaptic responses in VP and EP neurons projecting to LHb, whereas selective stimulation of STN terminals within VP induces place avoidance

(A) Patch-clamp electrophysiology to selectively record LHb-projecting EP and VP neurons that receive afferents from STN; Vglut2/ChR2 mice. Viral tracing strategy combining retro-AAV2-DIO-GFP into lateral habenula (LHb) and DIO-ChR2-mCherry virus into STN.

(legend continued on next page)

Based on these slice-derived results, the impact of selective STN terminal stimulation on aversion was next addressed in freely moving animals.

Selective stimulation of STN terminals within VP induces place avoidance

While selective EP stimulation is achievable in the *in vitro* setup (as above), the anatomical proximity between EP and STN makes selective manipulation of STN terminals within EP, without also affecting the STN, experimentally challenging in the *in vivo* context. Having identified connectivity between STN and VP, leading to activation in the LHb, we selected VP as the target area of interest and next investigated if photostimulation of STN terminals within VP is sufficient to drive the aversive avoidance behavior observed upon STN stimulation.

A new group of Pitx2-Cre mice were injected into the STN with the same viruses as previous mice but, this time, the fiber optic probes were bilaterally implanted above the VP to allow photostimulation of STN terminals (Figure 7N). These mice are referred to as $VP^{STN/ChR2}$ mice; controls are $VP^{STN/CTRL}$ mice (Figure 7). The same behavioral paradigms of emotional affect as implemented for STN photostimulation above was applied here for photostimulation of VP, leading to excitation of STN terminals.

In the Opto-OpenField, $VP^{STN/ChR2}$ mice showed a similar increase in grooming as when STN was photostimulated (Figure S7). In the Opto-Avoidance-EPM test, $VP^{STN/ChR2}$ mice showed decreased time spent and number of entries in the photostimulation-paired EPM arms, as shown by STN-stimulated mice (Figures 7P and S7).

In the Opto-RT-CPP paradigm (Figures 7Q and 7R), an active avoidance behavior to VP photostimulation was observed, with $VP^{STN/ChR2}$ mice visiting and spending significantly less time in the light-paired compartment (A) than the light-unpaired compartment (B) both during the 2 days of RT exposure and during the first conditioned test day (Figures 7R and S7), and reversing their preference in the reversal phase (Figures 7R and S7). Control mice showed an absence of photostimulation-dependent response throughout the sessions (Figures 7Q and S7).

Finally, when testing VP^{STN} mice in the Sugar-PR paradigm (Figures 7S and 7T), a similar response as obtained with STN-stimulated mice (STN^{Pitx2}/ChR2 and STN^{Vglut2}/ChR2) was obtained (Figures 7T and S7). The number of active and inactive NPs reached similar values during the last sessions of phase 2, and the average number of active NPs during phase 2 was significantly lower compared with both phase 1 and phase 3.

Taken together, the selective stimulation of STN-derived projection terminals within VP verified the responses observed upon STN stimulation, thus identifying the STN-VP connection in behavioral avoidance.

DISCUSSION

Taken together, this study takes advantage of four different molecular markers identified in mice to spatio-molecularly dissociate STN from pSTN, describe their distribution patterns qualitatively and quantitatively in mouse and macaque (Figures 1 and 2), and implement their promoters as drivers of Cre-recombinase in optogenetics-based neurocircuitry (Figures 3, 6, and 7) and behavior (Figures 4, 5, and 7) analysis focused on emotional affect. The main findings include: high level of translation between mouse and macaque (Figures 1 and 2), strikingly different efferent projections for STN vs. pSTN (Figure 3), identification of causality between STN excitation and aversive learning with an avoidance behavior (Figure 4) sufficiently potent to interrupt sugar self-administration (Figure 5), and the identification of STN stimulation-induced activity within STN and post-synaptic responses in LHb-projecting VP and EP neurons (Figures 6 and 7). Finally, the demonstration that STN terminal stimulation within VP causes similar behavioral avoidance as observed upon direct STN stimulation, thus identifying a possible aversion pathway involving the STN (Figure 7).

Dissociation of the heterogeneous STN and pSTN in aversion processing

By application of *Vglut2*, *Pitx2*, *PV*, and *Tac1* mRNA-directed probes in both mice and macaques, we re-confirm our previous demonstration of high level of selectivity for STN (*Pitx2*, *Vglut2*, *PV*) vs. pSTN (*Tac1*)[58] in the mouse, now including quantifications, and here reveal a high translational level for each marker between mouse and primate (Figures 1 and 2); findings validating the mouse as an experimental model for the primate in the present context. Taking advantage of this spatio-molecular

(B) Sagittal section; mCherry (magenta) and GFP (cyan).
(C and D) Confocal images. High magnification (upper quadrants): EP (C) and VP (D). *In vitro* recorded neurons filled with biocytin (BC) (yellow) (arrowheads) positive for GFP.
(E) EP (upper) and VP (bottom) neurons projecting to LHb (cyan) surrounded by STN terminals (magenta).
(F–I) Strategy representation for selectively patching EP (F) and VP (I) neurons projecting to LHb. Optic fiber placed above STN and axon terminals, respectively.
(G and J) Example traces of STN-EP/VP responses to 1 ms photostimulation with (yellow) or without (black) D-AP5+DNQX.
(H–K) Percentage of EP (H) and VP (K) cells responding to STN inputs.
(L) Amplitude, excitatory postsynaptic currents (EPSCs) between EP (n = 14) and VP (n = 6) cells.
(M) Latency, EPSC EP and VP cells.
(N) Behavior setup. STN-terminals stimulated in VP. Pitx2-Cre mice injected in STN and optic probes implanted above VP.
(O) YFP immunofluorescence; STN-derived projections in the VP.
(P) Opto-avoidance-EPM test. Time spent in arms: $VP^{STN/CTRL}$ (n = 8) vs. $VP^{STN/ChR2}$ (n = 14); representative heatmap: $VP^{STN/CTRL}$, $VP^{STN/ChR2}$.
(Q and R) Opto-RT-CPP; percentage time spent. Compartment A vs. compartment B: $VP^{STN/CTRL}$ (n = 8) (Q) and $VP^{STN/ChR2}$ (n = 14) (R). Blue circles (compartment A) and squares (compartment B) indicate photostimulation (Light-ON).
(S and T) Number of active vs. inactive nose-pokes: $VP^{STN/CTRL}$ (n = 4) (S) and $VP^{STN/ChR2}$ (n = 6) (T). Data were analyzed by MW-U test (I and M) and two-way RM ANOVA (P–T) followed by Šídák's multiple comparisons test (P, S, and T) or Tukey's multiple comparisons test (Q and R). Data expressed as mean ± SEM. *p < 0.05, **p < 0.01, ***p < 0.001. EP, entopeduncular nucleus; STN, subthalamic nucleus; LHb, lateral habenula; VP, ventral pallidum.

selectivity, we addressed the hypothesis that STN plays a role in aversion. The STN is classically associated with motor, associative, and limbic function; the limbic aspect of STN rather referring to reward-related functions.[73–75] In contrast, a causal role in aversion, and avoidance behavior, has not been proven. Studies in rodents showing that experimental STN-DBS induces different motivational responses depending on the nature of the reinforcers[30,76–79] and can reduce addictive behaviors[30,31,80] have identified a role for the STN in reward, relevant for addiction. Furthermore, low- and high-frequency stimulation (30 and 130 Hz, respectively) of the STN results in different outcome in models of addiction.[26,81] However, it has also been shown that STN lesioning in rats leads to altered emotional state in response to various rewarding and aversive stimuli.[77,80,82,83]

Classically, the ventro-medial aspect of the STN has been correlated with limbic function.[73] Often referred to as the "limbic tip," this is the part of the STN that is directly adjoined with pSTN, and where *Vglut2* shows higher intensity and PV^+ neurons are sparse; *Vglut2* and *PV* mRNAs showing almost opposite gradients (Figures 1 and 2). Using a combination of Cre-driver mice for which promoter activities were defined in the histological analysis to dissociate STN and pSTN, optogenetic excitation of either STN (STN^{Pitx2}/ChR2) or pSTN ($pSTN^{Tac1}$/ChR2) resulted in face grooming and place avoidance—directly associated with photostimulation (Opto-Avoidance-EPM and Opto-RT-CPP; RT phase). However, only STN excitation induced place avoidance upon exposure to photostimulation-paired cues (Opto-RT-CPP; test days), revealing a unique role for STN in aversive learning (Figure 4).

In a sugar-positive reinforcement paradigm (Sugar-PR), STN activation was sufficient to interrupt self-administration of sugar, whereas activation of pSTN did not hinder behavior to actively work for the reward (Figure 5). In this paradigm, results show that optogenetic stimulation of whole STN (*Vglut2*, *Pitx2*) causes an aversive phenotype, while stimulation of the pSTN (*Tac1*) induces a phenotype resembling appetitive behavior. Already previous work has associated pSTN with appetitive behavior (further discussed below), but this structure was recently implicated also in aversion.[45] Based on this data, the aversion response by STN and pSTN stimulation is demonstrated as distinctly different, and only STN mediates a learning component. Thus, the results allow a functional dissociation of the nature of the aversive response mediated by these two small and anatomically joined nuclei.

In terms of STN analysis, Vglut2/ChR2 mice showed more robust aversive response than Pitx2/ChR2 mice in the Opto-Avoidance-EPM and Opto-RT-CPP tests, but not in the Sugar-PR paradigm (Figures 4 and 5). Both *Vglut2* and *Pitx2* have been validated as relevant drivers of Cre-recombinase within STN.[48,49,50–52,84,85] However, with ample *Vglut2* in cellular densities immediately surrounding the STN, *Pitx2* as promoter for Cre-recombinase is more likely to direct selectivity to STN; we therefore reason that behaviors displayed by Pitx2/ChR2 mice are the most reliable representatives of STN-mediated behavior.

In contrast to STN, which has been the focus of attention in clinical and experimental research for decades, pSTN long remained largely unexplored. However, the past couple of years have seen a growing interest in this small structure, typically centered around food-intake behavior.[40,46,86] To date, pSTN has been implicated in a range of hypothalamic functions, including feeding, satiety, re-feeding, novelty response, fear, and appetitive as well as aversive responses.[37,40–45,86] The present study contributes with the finding that pSTN mice show mild aversion to optogenetic excitation in RT, but do not show conditioned aversion, and an appetitive rather than aversive behavior in the PR paradigm (Figures 4 and 5). Thus, while the aversive effect of STN stimulation identified here seems to be confirmed regardless of the experimental context, pSTN-mediated behavior shows more context dependence. Thus, the behavioral responses observed here corroborate our hypothesis that pSTN stimulation does not induce an aversive effect of comparable impact with that observed with STN stimulation.

Furthermore, not only complexity added by structures close to the STN, but also the functional heterogeneity *within* the STN is important to unravel experimentally. Here, we tested *PV*, identified as promoter active in a subpopulation of STN neurons in both rodents and primates.[55–59] Curiously, activation of the STN^{PV} subpopulation (PV/ChR2 mice) was similar to that of Pitx2/ChR2 mice in the Opto-RT-CPP test but caused only weak avoidance during the EPM-Avoidance test and no response in the Sugar-PR test (Figures 4 and 5). In the EPM-Avoidance and Sugar-PR test, any aversive effect must be strong enough to counteract the innate preference for sheltered areas and the rewarding characteristics of sugar, respectively, while in the Opto-RT-CPP the mouse can choose between two compartments of equal initial valence. In this context, the relatively smaller number of PV^+ neurons (compared with all of STN) may be sufficient to induce avoidance because other factors with greater valence are not involved. Another aspect to consider is the distribution pattern of PV^+ neurons. More abundant in dorsal than ventro-medial STN, the PV^+ subpopulation may not play a first-order role in limbic function, primarily associated with the limbic tip. Clearly, more work is needed to reveal the exact molecular identity of STN neurons engaging in avoidance-type behavior.

Neurocircuitry of behavioral aversion mediated by STN

In contrast to a recent interest in pallidal and habenular structures in aversion processing, the STN has been far less explored in this context. Based on the therapeutic effects of STN-DBS in PD, optogenetics in the STN has instead mainly been implemented in experimental animal models of PD.[65,87–94] The natural role of STN has remained more poorly investigated. However, recent studies have explored the STN in locomotor control, action selection, and stopping of cognitive processes.[48,50,51] The STN, which receives inputs from cortical regions supporting hedonic processing,[74,95–97] might play a modulatory role in decision-making in response to aversive conditions.

The present results place the STN in the context of aversion neurocircuitry. Several of the structures recognized in aversive processing receive projections from the STN. These include GPi/EP and VP, as confirmed here (Figure 3), and carefully described in previous work.[2,6,48,69–72,98] Both EP and VP project to LHb, which, in turn, has proven responsible for mediating aversive behavior. For instance, optogenetic stimulation of glutamatergic neurons of the EP,[70,71] VP,[69,72] and LH[99,100] projecting to the LHb induces place avoidance. Based on previous work defining a role for VP in integrating aversive and rewarding information,[69,101–106] VP might represent a plausible connecting

structure bridging STN with LHb. VP is primarily GABAergic, but a recent study demonstrated the presence of glutamatergic VP neurons projecting to LHb.[69,72] Furthermore, this glutamatergic VP subpopulation receives projections from the STN, and selective stimulation of glutamatergic VP neurons has been shown to evoke EPSCs in LHb and to induce RT avoidance.[72] Our findings identified aversion upon stimulation of either STN cell bodies or STN terminals in VP (Figures 4, 5, and 7). Using *in vivo* extracellular recordings, we confirmed activational response of STN neurons upon STN-directed photostimulation and demonstrated that stimulation of STN neurons drives neuronal activity in the LHb, while *ex vivo* patch clamping of $VP^{STN-LHb}$ and $EP^{STN-LHb}$ neurons allowed the identification of excitatory post-synaptic responses during STN photostimulation (Figures 6 and 7). Together, these results provide support for a pathway from STN via VP/EP toward LHb. However, with substantial projections between the STN and additional brain areas (Figure 3), including midbrain dopaminergic neurons of SNc and ventral tegmental area, that also have been associated with aversion,[107,108] additional studies will be required to fully define the neurocircuitry of STN-mediated aversion.

Clinical importance of understanding the role of STN in behavioral regulation

The STN is best known for its role in movement inhibition in PD. However, PD contains both motor and non-motor symptom domains.[109–111] In PD, the STN shows aberrant firing activity, which exacerbates movement inability induced by loss of dopamine. STN-DBS improves PD motor symptoms[112–114] demonstrating the crucial role of STN in voluntary movement. However, a major challenge with STN-DBS is the emergence of side effects, some of which resemble non-motor symptoms, including low mood state.[115,116] Direct causality between STN excitation and behavioral aversion might be important in this context. Also the proximity of STN to the multi-faceted pSTN may be clinically relevant in terms of side effects upon STN-DBS. Anatomical-functional dissociation of STN and pSTN in both the rodent and primate, as initiated here, is important for better understanding of this heterogeneous brain area.

In addition to PD, tremor, dystonia, and Tourette syndrome, STN-DBS is applied in treatment-resistant OCD.[18,25,117–119] High-frequency stimulation of the antero-medial STN has been correlated with hypomania[120] and shown to alleviate OCD.[5] However, some OCD patients are unresponsive to STN-DBS.[18,121] A recent study focused on psychosurgical DBS targets argued for the importance of precise characterization of the morphological organization of the subthalamic area in the primate brain to improve success rate in treatment of psychiatric disorders, including OCD and depression.[122] By addressing gene expression patterns within STN and its immediate surroundings in the macaque monkey, the current results provide enhanced insight into the molecular, cellular, and anatomical organization of this brain region.

In the context of compulsive behavior, excessive grooming was observed upon excitation of either STN or pSTN, with somewhat different timing in response to the stimulation (Figure S3). A direct correlation between STN excitation and grooming behavior was first reported only a couple of years ago.[48,49] While grooming is a natural behavior for rodents, accentuated grooming behavior may be a sign of distress.[63,64] Also certain compulsions in humans, such as excessive self-grooming, have been suggested to manifest behavioral repetitions in attempts to relieve anxiety and/or aversion caused by strongly unpleasant sensations.[123] Accordingly, stereotypic grooming is implemented as one of several criteria for compulsive behavior in rodent models of OCD.[124–126] The data presented here provide compelling causality between selective optogenetic excitation of either STN or pSTN and compulsive grooming. Considering the putative circuitry of this behavioral display, it is worth noting that, while STN (*Pitx2*) and pSTN (*Tac1*) show vastly different projection patterns, two target areas stand out as identical (VP and SNc) (Figure 3), motivating further analysis in the context of compulsive behavior.

In summary, this study identifies a role for the STN in aversion and aversive learning. The findings provide a neurobiological framework for STN in emotional affect with implications for neurological and neuropsychiatric disorders in which STN dysfunction is a critical brain pathology. The study also found that STN-mediated aversion is distinct from pSTN-driven affect. The results should be relevant when applying STN as a target for therapeutic intervention, and to possibilities of improving precision toward discrete symptoms.

Limitations of the study

Injection site, probe placement, and amount of mice. Antidromic spiking of STN neurons cannot be excluded in the terminal stimulation experiment. Lack of response in the negative reinforcement paradigm likely reflects an effect of lost motivation that should be further explored.

STAR★METHODS

Detailed methods are provided in the online version of this paper and include the following:

- KEY RESOURCES TABLE
- RESOURCE AVAILABILITY
  - Lead contact
  - Materials availability
  - Data and code availability
- EXPERIMENTAL MODEL AND STUDY PARTICIPANT DETAILS
  - Cre-recombinase mouse strains
  - Macaque brain tissue
- METHOD DETAILS
  - Fluorescent *in situ* hybridization (FISH) histochemistry
  - Stereotaxic virus injection and fiber optic probe implantation
  - Single-cell extracellular recordings
  - *Ex vivo* electrophysiology
  - Electrophysiological recordings
  - Pharmacology
  - Behavioral testing
  - Criteria for exclusion from the analysis
  - Post-injection histological analysis
- QUANTIFICATION AND STATISTICAL ANALYSIS

SUPPLEMENTAL INFORMATION

Supplemental information can be found online at https://doi.org/10.1016/j.celrep.2023.113328.

ACKNOWLEDGMENTS

We thank James Martin, Baylor College of Medicine, and Ole Kiehn, University of Copenhagen, for generously providing Pitx2-Cre and Vglut2-Cre mice, respectively; Marie Englund, Uppsala University, for biopsy genotyping; and Chantal François, Université de Sorbonne, Paris, for macaque tissue. Funding sources: Vetenskapsrådet, Hjärnfonden, Parkinsonfonden, Research foundations of Bertil Hållsten, Zoologiska, and Åhlén (to Å.W.-M); OE&Edla Johansson (to G.P.S). This work has benefited from a government grant awarded to University of Bordeaux as an Initiative of Excellence under the France 2030 plan (to J.B. and Å.W.-M.) and research sabbatical grants from Uppsala University and Wenner-Gren Stiftelserna (to Å.W.-M.). This work was also funded by Aligning Science Across Parkinson's (ASAP-020600; Lead PI R. Awatramani) through the Michael J. Fox Foundation for Parkinson's Research (MJFF) (to Å.W.-M.). Partners in this network are thanked for constructive feedback. For the purpose of open access, the authors have applied a CC BY public copyright license to all Author Accepted Manuscripts arising from this submission. The funders had no role in study design, data collection and analysis, decision to publish, or preparation of the paper.

AUTHOR CONTRIBUTIONS

Conceptualization, G.P.S., J.B., F.G., and Å.W.-M.; methodology, G.P.S., J.B., F.G., S.D., and Å.W.-M.; formal analysis, G.P.S., S.D., and J.B.; investigation, G.P.S., A.G., B.V., L.D.-Z., A.R., E.R., S.D., and Å.W.-M.; writing – original draft, Å.W.-M.; writing – review & editing, G.P.S., F.G., J.B., and Å.W.-M.; visualization, G.P.S., A.G., L.D.-Z., A.R., E.R., S.D., J.B., F.G., and Å.W.-M.; supervision, F.G., J.B., and Å.W.-M.; project administration, Å.W.-M.; funding acquisition, J.B. and Å.W.-M.

DECLARATION OF INTERESTS

S.D. is the owner of Oramacell, Paris, France.

Received: February 27, 2023
Revised: July 28, 2023
Accepted: October 8, 2023

REFERENCES

1. Albin, R.L., Young, A.B., and Penney, J.B. (1989). The functional anatomy of basal ganglia disorders. Trends Neurosci. *12*, 366–375. https://doi.org/10.1016/0166-2236(89)90074-X.
2. Alexander, G.E., and Crutcher, M.D. (1990). Functional architecture of basal ganglia circuits: neural substrates of parallel processing. Trends Neurosci. *13*, 266–271. https://doi.org/10.1016/0166-2236(90)90107-L.
3. Benabid, A.L., Chabardes, S., Mitrofanis, J., and Pollak, P. (2009). Deep brain stimulation of the subthalamic nucleus for the treatment of Parkinson's disease. Lancet Neurol. *8*, 67–81. https://doi.org/10.1016/S1474-4422(08)70291-6.
4. DeLong, M.R. (1990). Primate models of movement disorders of basal ganglia origin. Trends Neurosci. *13*, 281–285. https://doi.org/10.1016/0166-2236(90)90110-V.
5. Mallet, L., Schüpbach, M., N'Diaye, K., Remy, P., Bardinet, E., Czernecki, V., Welter, M.-L., Pelissolo, A., Ruberg, M., Agid, Y., and Yelnik, J. (2007). Stimulation of subterritories of the subthalamic nucleus reveals its role in the integration of the emotional and motor aspects of behavior. Proc. Natl. Acad. Sci. USA *104*, 10661–10666. https://doi.org/10.1073/pnas.0610849104.
6. Nambu, A., Tokuno, H., and Takada, M. (2002). Functional significance of the cortico–subthalamo–pallidal 'hyperdirect' pathway. Neurosci. Res. *43*, 111–117. https://doi.org/10.1016/S0168-0102(02)00027-5.
7. Nougaret, S., Baunez, C., and Ravel, S. (2022). Neurons in the Monkey's Subthalamic Nucleus Differentially Encode Motivation and Effort. J. Neurosci. *42*, 2539–2551. https://doi.org/10.1523/JNEUROSCI.0281-21.2021.
8. Sano, H., Chiken, S., Hikida, T., Kobayashi, K., and Nambu, A. (2013). Signals through the Striatopallidal Indirect Pathway Stop Movements by Phasic Excitation in the Substantia Nigra. J. Neurosci. *33*, 7583–7594. https://doi.org/10.1523/JNEUROSCI.4932-12.2013.
9. Schmidt, R., and Berke, J.D. (2017). A Pause-then-Cancel model of stopping: evidence from basal ganglia neurophysiology. Philos. Trans. R. Soc. Lond. B Biol. Sci. *372*, 20160202. https://doi.org/10.1098/rstb.2016.0202.
10. Sieger, T., Serranová, T., Růžička, F., Vostatek, P., Wild, J., Šťastná, D., Bonnet, C., Novák, D., Růžička, E., Urgošík, D., and Jech, R. (2015). Distinct populations of neurons respond to emotional valence and arousal in the human subthalamic nucleus. Proc. Natl. Acad. Sci. USA *112*, 3116–3121. https://doi.org/10.1073/pnas.1410709112.
11. Voon, V., Droux, F., Morris, L., Chabardes, S., Bougerol, T., David, O., Krack, P., and Polosan, M. (2017). Decisional impulsivity and the associative-limbic subthalamic nucleus in obsessive-compulsive disorder: stimulation and connectivity. Brain *140*, 442–456. https://doi.org/10.1093/brain/aww309.
12. Voon, V., Kubu, C., Krack, P., Houeto, J.-L., and Tröster, A.I. (2006). Deep brain stimulation: Neuropsychological and neuropsychiatric issues. Mov. Disord. *21*, S305–S327. https://doi.org/10.1002/mds.20963.
13. Witt, K., Daniels, C., Reiff, J., Krack, P., Volkmann, J., Pinsker, M.O., Krause, M., Tronnier, V., Kloss, M., Schnitzler, A., et al. (2008). Neuropsychological and psychiatric changes after deep brain stimulation for Parkinson's disease: a randomised, multicentre study. Lancet Neurol. *7*, 605–614. https://doi.org/10.1016/S1474-4422(08)70114-5.
14. Chu, H.-Y., Atherton, J.F., Wokosin, D., Surmeier, D.J., and Bevan, M.D. (2015). Heterosynaptic Regulation of External Globus Pallidus Inputs to the Subthalamic Nucleus by the Motor Cortex. Neuron *85*, 364–376. https://doi.org/10.1016/j.neuron.2014.12.022.
15. Smith, Y., Bevan, M.D., Shink, E., and Bolam, J.P. (1998). Microcircuitry of the direct and indirect pathways of the basal ganglia. Neuroscience *86*, 353.
16. Bolam, J.P., Hanley, J.J., Booth, P.A., and Bevan, M.D. (2000). Synaptic organisation of the basal ganglia. J. Anat. *196*, 527–542. https://doi.org/10.1046/j.1469-7580.2000.19640527.x.
17. Vila, M., Périer, C., Féger, J., Yelnik, J., Faucheux, B., Ruberg, M., Raisman-Vozari, R., Agid, Y., and Hirsch, E.C. (2000). Evolution of changes in neuronal activity in the subthalamic nucleus of rats with unilateral lesion of the substantia nigra assessed by metabolic and electrophysiological measurements: Subthalamic nucleus activity in parkinsonism. Eur. J. Neurosci. *12*, 337–344. https://doi.org/10.1046/j.1460-9568.2000.00901.x.
18. Mallet, L., Polosan, M., Jaafari, N., Baup, N., Welter, M.-L., Fontaine, D., du Montcel, S.T., Yelnik, J., Chéreau, I., Arbus, C., et al. (2008). Subthalamic Nucleus Stimulation in Severe Obsessive–Compulsive Disorder. N. Engl. J. Med. *359*, 2121–2134. https://doi.org/10.1056/NEJMoa0708514.
19. Dickson, D.W., Ahmed, Z., Algom, A.A., Tsuboi, Y., and Josephs, K.A. (2010). Neuropathology of variants of progressive supranuclear palsy. Curr. Opin. Neurol. *23*, 394–400. https://doi.org/10.1097/WCO.0b013e32833be924.
20. Lange, H., Thörner, G., Hopf, A., and Schröder, K.F. (1976). Morphometric studies of the neuropathological changes in choreatic diseases. J. Neurol. Sci. *28*, 401–425. https://doi.org/10.1016/0022-510X(76)90114-3.

21. Atherton, J.F., McIver, E.L., Mullen, M.R., Wokosin, D.L., Surmeier, D.J., and Bevan, M.D. (2016). Early dysfunction and progressive degeneration of the subthalamic nucleus in mouse models of Huntington's disease. Elife *5*, e21616. https://doi.org/10.7554/eLife.21616.

22. Tyagi, H., Apergis-Schoute, A.M., Akram, H., Foltynie, T., Limousin, P., Drummond, L.M., Fineberg, N.A., Matthews, K., Jahanshahi, M., Robbins, T.W., et al. (2019). A Randomized Trial Directly Comparing Ventral Capsule and Anteromedial Subthalamic Nucleus Stimulation in Obsessive-Compulsive Disorder: Clinical and Imaging Evidence for Dissociable Effects. Biol. Psychiatry *85*, 726–734. https://doi.org/10.1016/j.biopsych.2019.01.017.

23. Mosley, P.E., and Akram, H. (2021). Neuropsychiatric effects of subthalamic deep brain stimulation. In Handbook of Clinical Neurology (Elsevier), pp. 417–431. https://doi.org/10.1016/B978-0-12-820107-7.00026-4.

24. Dai, L., Xu, W., Song, Y., Huang, P., Li, N., Hollunder, B., Horn, A., Wu, Y., Zhang, C., Sun, B., and Li, D. (2022). Subthalamic deep brain stimulation for refractory Gilles de la Tourette's syndrome: clinical outcome and functional connectivity. J. Neurol. *269*, 6116–6126. https://doi.org/10.1007/s00415-022-11266-w.

25. Vissani, M., Cordella, R., Micera, S., Eleopra, R., Romito, L.M., and Mazzoni, A. (2019). Spatio-temporal structure of single neuron subthalamic activity identifies DBS target for anesthetized Tourette syndrome patients. J. Neural. Eng. *16*, 066011. https://doi.org/10.1088/1741-2552/ab37b4.

26. Pelloux, Y., Degoulet, M., Tiran-Cappello, A., Cohen, C., Lardeux, S., George, O., Koob, G.F., Ahmed, S.H., and Baunez, C. (2018). Subthalamic nucleus high frequency stimulation prevents and reverses escalated cocaine use. Mol. Psychiatry *23*, 2266–2276. https://doi.org/10.1038/s41380-018-0080-y.

27. Y. Pelloux, C. Baunez, and M. Torregrossa, eds. (2019). Harnessing Circuits for the Treatment of Addictive Disorders (Elsevier: Neural Mechanisms of Addiction), pp. 271–285. https://doi.org/10.1016/B978-0-12-812202-0.00019-1.

28. Pelloux, Y., and Baunez, C. (2017). Targeting the subthalamic nucleus in a preclinical model of alcohol use disorder. Psychopharmacology *234*, 2127–2137. https://doi.org/10.1007/s00213-017-4618-5.

29. Pelloux, Y., and Baunez, C. (2013). Deep brain stimulation for addiction: why the subthalamic nucleus should be favored. Curr. Opin. Neurobiol. *23*, 713–720. https://doi.org/10.1016/j.conb.2013.02.016.

30. Rouaud, T., Lardeux, S., Panayotis, N., Paleressompoulle, D., Cador, M., and Baunez, C. (2010). Reducing the desire for cocaine with subthalamic nucleus deep brain stimulation. Proc. Natl. Acad. Sci. USA *107*, 1196–1200. https://doi.org/10.1073/pnas.0908189107.

31. Wade, C.L., Kallupi, M., Hernandez, D.O., Breysse, E., de Guglielmo, G., Crawford, E., Koob, G.F., Schweitzer, P., Baunez, C., and George, O. (2017). High-Frequency Stimulation of the Subthalamic Nucleus Blocks Compulsive-Like Re-Escalation of Heroin Taking in Rats. Neuropsychopharmacology *42*, 1850–1859. https://doi.org/10.1038/npp.2016.270.

32. Volkmann, J., Daniels, C., and Witt, K. (2010). Neuropsychiatric effects of subthalamic neurostimulation in Parkinson disease. Nat. Rev. Neurol. *6*, 487–498. https://doi.org/10.1038/nrneurol.2010.111.

33. Gerfen, C.R., and Bolam, J.P. (2010). The Neuroanatomical Organization of the Basal Ganglia. In Handbook of Behavioral Neuroscience (Elsevier), pp. 3–28. https://doi.org/10.1016/B978-0-12-374767-9.00001-9.

34. Goto, M., and Swanson, L.W. (2004). Axonal projections from the parasubthalamic nucleus. J. Comp. Neurol. *469*, 581–607. https://doi.org/10.1002/cne.11036.

35. Kita, T., Shigematsu, N., and Kita, H. (2016). Intralaminar and tectal projections to the subthalamus in the rat. Eur. J. Neurosci. *44*, 2899–2908. https://doi.org/10.1111/ejn.13413.

36. Parent, A., and Hazrati, L.-N. (1995). Functional anatomy of the basal ganglia. II. The place of subthalamic nucleus and external pallidium in basal ganglia circuitry. Brain Res. Rev. *20*, 128–154. https://doi.org/10.1016/0165-0173(94)00008-D.

37. Shah, T., Dunning, J.L., and Contet, C. (2022). At the heart of the interoception network: Influence of the parasubthalamic nucleus on autonomic functions and motivated behaviors. Neuropharmacology *204*, 108906. https://doi.org/10.1016/j.neuropharm.2021.108906.

38. Blomstedt, P., Stenmark Persson, R., Hariz, G.-M., Linder, J., Fredricks, A., Häggström, B., Philipsson, J., Forsgren, L., and Hariz, M. (2018). Deep brain stimulation in the caudal zona incerta versus best medical treatment in patients with Parkinson's disease: a randomised blinded evaluation. J. Neurol. Neurosurg. Psychiatry *89*, 710–716. https://doi.org/10.1136/jnnp-2017-317219.

39. De Marco, R., Bhargava, D., Macerollo, A., and Osman-Farah, J. (2020). Could ZI have a role in DBS for Parkinson's Disease? An observational study to optimize DBS target localization. J. Clin. Neurosci. *77*, 89–93. https://doi.org/10.1016/j.jocn.2020.05.029.

40. Barbier, M., Chometton, S., Pautrat, A., Miguet-Alfonsi, C., Datiche, F., Gascuel, J., Fellmann, D., Peterschmitt, Y., Coizet, V., and Risold, P.-Y. (2020). A basal ganglia-like cortical–amygdalar–hypothalamic network mediates feeding behavior. Proc. Natl. Acad. Sci. USA *117*, 15967–15976. https://doi.org/10.1073/pnas.2004914117.

41. Bowen, A.J., Chen, J.Y., Huang, Y.W., Baertsch, N.A., Park, S., and Palmiter, R.D. (2020). Dissociable control of unconditioned responses and associative fear learning by parabrachial CGRP neurons. Elife *9*, e59799. https://doi.org/10.7554/eLife.59799.

42. Kim, J.H., Kromm, G.H., Barnhill, O.K., Sperber, J., Heuer, L.B., Loomis, S., Newman, M.C., Han, K., Gulamali, F.F., Legan, T.B., et al. (2022). A discrete parasubthalamic nucleus subpopulation plays a critical role in appetite suppression. Elife *11*, e75470. https://doi.org/10.7554/eLife.75470.

43. Liu, C., Lee, C.-Y., Asher, G., Cao, L., Terakoshi, Y., Cao, P., Kobayakawa, R., Kobayakawa, K., Sakurai, K., and Liu, Q. (2021). Posterior subthalamic nucleus (PSTh) mediates innate fear-associated hypothermia in mice. Nat. Commun. *12*, 2648. https://doi.org/10.1038/s41467-021-22914-6.

44. Sanchez, M.R., Wang, Y., Cho, T.S., Schnapp, W.I., Schmit, M.B., Fang, C., and Cai, H. (2022). Dissecting a disynaptic central amygdala-parasubthalamic nucleus neural circuit that mediates cholecystokinin-induced eating suppression. Mol. Metab. *58*, 101443. https://doi.org/10.1016/j.molmet.2022.101443.

45. Zhang, X., and van den Pol, A.N. (2017). Rapid binge-like eating and body weight gain driven by zona incerta GABA neuron activation. Science *356*, 853–859. https://doi.org/10.1126/science.aam7100.

46. Hansen, H.H., Perens, J., Roostalu, U., Skytte, J.L., Salinas, C.G., Barkholt, P., Thorbek, D.D., Rigbolt, K.T.G., Vrang, N., Jelsing, J., and Hecksher-Sørensen, J. (2021). Whole-brain activation signatures of weight-lowering drugs. Mol. Metab. *47*, 101171. https://doi.org/10.1016/j.molmet.2021.101171.

47. Nambu, A., Tokuno, H., Hamada, I., Kita, H., Imanishi, M., Akazawa, T., Ikeuchi, Y., and Hasegawa, N. (2000). Excitatory Cortical Inputs to Pallidal Neurons Via the Subthalamic Nucleus in the Monkey. J. Neurophysiol. *84*, 289–300. https://doi.org/10.1152/jn.2000.84.1.289.

48. Guillaumin, A., Serra, G.P., Georges, F., and Wallén-Mackenzie, Å. (2021). Experimental investigation into the role of the subthalamic nucleus (STN) in motor control using optogenetics in mice. Brain Res. *1755*, 147226. https://doi.org/10.1016/j.brainres.2020.147226.

49. Parolari, L., Schneeberger, M., Heintz, N., and Friedman, J.M. (2021). Functional analysis of distinct populations of subthalamic nucleus neurons on Parkinson's disease and OCD-like behaviors in mice. Mol. Psychiatry *26*, 7029–7046. https://doi.org/10.1038/s41380-021-01162-6.

50. Fife, K.H., Gutierrez-Reed, N.A., Zell, V., Bailly, J., Lewis, C.M., Aron, A.R., and Hnasko, T.S. (2017). Causal role for the subthalamic nucleus in interrupting behavior. Elife *6*, e27689. https://doi.org/10.7554/eLife.27689.

51. Heston, J., Friedman, A., Baqai, M., Bavafa, N., Aron, A.R., and Hnasko, T.S. (2020). Activation of Subthalamic Nucleus Stop Circuit Disrupts Cognitive Performance. eNeuro *7*, ENEURO.0159, 20.2020. https://doi.org/10.1523/ENEURO.0159-20.2020.

52. Schweizer, N., Pupe, S., Arvidsson, E., Nordenankar, K., Smith-Anttila, C.J.A., Mahmoudi, S., Andrén, A., Dumas, S., Rajagopalan, A., Lévesque, D., et al. (2014). Limiting glutamate transmission in a Vglut2-expressing subpopulation of the subthalamic nucleus is sufficient to cause hyperlocomotion. Proc. Natl. Acad. Sci. USA *111*, 7837–7842. https://doi.org/10.1073/pnas.1323499111.

53. Martin, D.M., Skidmore, J.M., Philips, S.T., Vieira, C., Gage, P.J., Condie, B.G., Raphael, Y., Martinez, S., and Camper, S.A. (2004). PITX2 is required for normal development of neurons in the mouse subthalamic nucleus and midbrain. Dev. Biol. *267*, 93–108. https://doi.org/10.1016/j.ydbio.2003.10.035.

54. Skidmore, J.M., Cramer, J.D., Martin, J.F., and Martin, D.M. (2008). Cre fate mapping reveals lineage specific defects in neuronal migration with loss of Pitx2 function in the developing mouse hypothalamus and subthalamic nucleus. Mol. Cell. Neurosci. *37*, 696–707. https://doi.org/10.1016/j.mcn.2007.12.015.

55. Alkemade, A., de Hollander, G., Miletic, S., Keuken, M.C., Balesar, R., de Boer, O., Swaab, D.F., and Forstmann, B.U. (2019). The functional microscopic neuroanatomy of the human subthalamic nucleus. Brain Struct. Funct. *224*, 3213–3227. https://doi.org/10.1007/s00429-019-01960-3.

56. Jeon, H., Lee, H., Kwon, D.-H., Kim, J., Tanaka-Yamamoto, K., Yook, J.S., Feng, L., Park, H.R., Lim, Y.H., Cho, Z.-H., et al. (2022). Topographic connectivity and cellular profiling reveal detailed input pathways and functionally distinct cell types in the subthalamic nucleus. Cell Rep. *38*, 110439. https://doi.org/10.1016/j.celrep.2022.110439.

57. Lévesque, J.C., and Parent, A. (2005). GABAergic interneurons in human subthalamic nucleus. Mov. Disord. *20*, 574–584. https://doi.org/10.1002/mds.20374.

58. Wallén-Mackenzie, Å., Dumas, S., Papathanou, M., Martis Thiele, M.M., Vlcek, B., König, N., and Björklund, Å.K. (2020). Spatio-molecular domains identified in the mouse subthalamic nucleus and neighboring glutamatergic and GABAergic brain structures. Commun. Biol. *3*, 338. https://doi.org/10.1038/s42003-020-1028-8.

59. Wu, X.H., Song, J.J., Faull, R.L.M., and Waldvogel, H.J. (2018). GABA $_{A}$ and GABA $_{B}$ receptor subunit localization on neurochemically identified neurons of the human subthalamic nucleus. J. Comp. Neurol. *526*, 803–823. https://doi.org/10.1002/cne.24368.

60. Franklin, K.B.J., and Paxinos, G. (2008). The Mouse Brain in Stereotaxic Coordinates Compact 3 (Elsevier, Academic Press).

61. Berridge, K.C., Aldridge, J.W., Houchard, K.R., and Zhuang, X. (2005). Sequential super-stereotypy of an instinctive fixed action pattern in hyper-dopaminergic mutant mice: a model of obsessive compulsive disorder and Tourette's. BMC Biol. *3*, 4. https://doi.org/10.1186/1741-7007-3-4.

62. Fentress, J.C. (1988). Expressive Contexts, Fine Structure, and Central Mediation of Rodent Grooming. Ann. N. Y. Acad. Sci. *525*, 18–26. https://doi.org/10.1111/j.1749-6632.1988.tb38592.x.

63. Kalueff, A.V., Stewart, A.M., Song, C., Berridge, K.C., Graybiel, A.M., and Fentress, J.C. (2016). Neurobiology of rodent self-grooming and its value for translational neuroscience. Nat. Rev. Neurosci. *17*, 45–59. https://doi.org/10.1038/nrn.2015.8.

64. Kalueff, A.V., Wheaton, M., and Murphy, D.L. (2007). What's wrong with my mouse model? Behav. Brain Res. *179*, 1–18. https://doi.org/10.1016/j.bbr.2007.01.023.

65. Gradinaru, V., Mogri, M., Thompson, K.R., Henderson, J.M., and Deisseroth, K. (2009). Optical Deconstruction of Parkinsonian Neural Circuitry. Science *324*, 354–359. https://doi.org/10.1126/science.1167093.

66. Witten, I.B., Lin, S.-C., Brodsky, M., Prakash, R., Diester, I., Anikeeva, P., Gradinaru, V., Ramakrishnan, C., and Deisseroth, K. (2010). Cholinergic Interneurons Control Local Circuit Activity and Cocaine Conditioning. Science *330*, 1677–1681. https://doi.org/10.1126/science.1193771.

67. Hartung, H., Tan, S.K.H., Temel, Y., and Sharp, T. (2016). High-frequency stimulation of the subthalamic nucleus modulates neuronal activity in the lateral habenula nucleus. Eur. J. Neurosci. *44*, 2698–2707. https://doi.org/10.1111/ejn.13397.

68. Tan, S.K.H., Janssen, M.L.F., Jahanshahi, A., Chouliaras, L., Visser-Vandewalle, V., Lim, L.W., Steinbusch, H.W.M., Sharp, T., and Temel, Y. (2011). High frequency stimulation of the subthalamic nucleus increases c-fos immunoreactivity in the dorsal raphe nucleus and afferent brain regions. J. Psychiatr. Res. *45*, 1307–1315. https://doi.org/10.1016/j.jpsychires.2011.04.011.

69. Faget, L., Zell, V., Souter, E., McPherson, A., Ressler, R., Gutierrez-Reed, N., Yoo, J.H., Dulcis, D., and Hnasko, T.S. (2018). Opponent control of behavioral reinforcement by inhibitory and excitatory projections from the ventral pallidum. Nat. Commun. *9*, 849. https://doi.org/10.1038/s41467-018-03125-y.

70. Shabel, S.J., Proulx, C.D., Trias, A., Murphy, R.T., and Malinow, R. (2012). Input to the Lateral Habenula from the Basal Ganglia Is Excitatory, Aversive, and Suppressed by Serotonin. Neuron *74*, 475–481. https://doi.org/10.1016/j.neuron.2012.02.037.

71. Stephenson-Jones, M., Yu, K., Ahrens, S., Tucciarone, J.M., van Huijstee, A.N., Mejia, L.A., Penzo, M.A., Tai, L.-H., Wilbrecht, L., and Li, B. (2016). A basal ganglia circuit for evaluating action outcomes. Nature *539*, 289–293. https://doi.org/10.1038/nature19845.

72. Tooley, J., Marconi, L., Alipio, J.B., Matikainen-Ankney, B., Georgiou, P., Kravitz, A.V., and Creed, M.C. (2018). Glutamatergic Ventral Pallidal Neurons Modulate Activity of the Habenula–Tegmental Circuitry and Constrain Reward Seeking. Biol. Psychiatry *83*, 1012–1023. https://doi.org/10.1016/j.biopsych.2018.01.003.

73. Alkemade, A., Schnitzler, A., and Forstmann, B.U. (2015). Topographic organization of the human and non-human primate subthalamic nucleus. Brain Struct. Funct. *220*, 3075–3086. https://doi.org/10.1007/s00429-015-1047-2.

74. Haynes, W.I.A., and Haber, S.N. (2013). The Organization of Prefrontal-Subthalamic Inputs in Primates Provides an Anatomical Substrate for Both Functional Specificity and Integration: Implications for Basal Ganglia Models and Deep Brain Stimulation. J. Neurosci. *33*, 4804–4814. https://doi.org/10.1523/JNEUROSCI.4674-12.2013.

75. Yelnik, J., Bardinet, E., Dormont, D., Malandain, G., Ourselin, S., Tandé, D., Karachi, C., Ayache, N., Cornu, P., and Agid, Y. (2007). A three-dimensional, histological and deformable atlas of the human basal ganglia. I. Atlas construction based on immunohistochemical and MRI data. Neuroimage *34*, 618–638. https://doi.org/10.1016/j.neuroimage.2006.09.026.

76. Anderson, C., Sheppard, D., and Dorval, A.D. (2020). Parkinsonism and subthalamic deep brain stimulation dysregulate behavioral motivation in a rodent model. Brain Res. *1736*, 146776. https://doi.org/10.1016/j.brainres.2020.146776.

77. Baunez, C., Amalric, M., and Robbins, T.W. (2002). Enhanced Food-Related Motivation after Bilateral Lesions of the Subthalamic Nucleus. J. Neurosci. *22*, 562–568. https://doi.org/10.1523/JNEUROSCI.22-02-00562.2002.

78. Darbaky, Y., Baunez, C., Arecchi, P., Legallet, E., and Apicella, P. (2005). Reward-related neuronal activity in the subthalamic nucleus of the monkey. Neuroreport *16*, 1241–1244. https://doi.org/10.1097/00001756-200508010-00022.

79. Vachez, Y., Carcenac, C., Magnard, R., Kerkerian Le Goff, L., Salin, P., Savasta, M., Carnicella, S., and Boulet, S. (2020). Subthalamic Nucleus Stimulation Impairs Motivation: Implication for Apathy in Parkinson's Disease. Mov. Disord. *35*, 616–628. https://doi.org/10.1002/mds.27953.

80. Lardeux, S., and Baunez, C. (2008). Alcohol Preference Influences the Subthalamic Nucleus Control on Motivation for Alcohol in Rats.

Neuropsychopharmacology *33*, 634–642. https://doi.org/10.1038/sj.npp.1301432.

81. Degoulet, M., Tiran-Cappello, A., Combrisson, E., Baunez, C., and Pelloux, Y. (2021). Subthalamic low-frequency oscillations predict vulnerability to cocaine addiction. Proc. Natl. Acad. Sci. USA *118*, e2024121118. https://doi.org/10.1073/pnas.2024121118.
82. Baunez, C., Dias, C., Cador, M., and Amalric, M. (2005). The subthalamic nucleus exerts opposite control on cocaine and "natural" rewards. Nat. Neurosci. *8*, 484–489. https://doi.org/10.1038/nn1429.
83. Pelloux, Y., Meffre, J., Giorla, E., and Baunez, C. (2014). The subthalamic nucleus keeps you high on emotion: behavioral consequences of its inactivation. Front. Behav. Neurosci. *8*, 414. https://doi.org/10.3389/fnbeh.2014.00414.
84. Schweizer, N., Viereckel, T., Smith-Anttila, C.J., Nordenankar, K., Arvidsson, E., Mahmoudi, S., Zampera, A., Wärner Jonsson, H., Bergquist, J., Lévesque, D., et al. (2016). Reduced Vglut2/Slc17a6 Gene Expression Levels throughout the Mouse Subthalamic Nucleus Cause Cell Loss and Structural Disorganization Followed by Increased Motor Activity and Decreased Sugar Consumption. eNeuro *3*, ENEURO.0264. https://doi.org/10.1523/ENEURO.0264-16.2016.
85. Viereckel, T., Konradsson-Geuken, Å., and Wallén-Mackenzie, Å. (2018). Validated multi-step approach for in vivo recording and analysis of optogenetically evoked glutamate in the mouse globus pallidus. J. Neurochem. *145*, 125–138. https://doi.org/10.1111/jnc.14288.
86. Dunning, J.L., Lopez, C., Krull, C., Kreifeldt, M., Angelo, M., Ramakrishnan, C., Deisseroth, K., and Contet, C. (2023). The parasubthalamic nucleus refeeding ensemble delays feeding initiation. bioRxiv. https://doi.org/10.1101/2023.01.28.525750.
87. Pamukcu, A., Cui, Q., Xenias, H.S., Berceau, B.L., Augustine, E.C., Fan, I., Chalasani, S., Hantman, A.W., Lerner, T.N., Boca, S.M., and Chan, C.S. (2020). Parvalbumin $^{+}$ and Npas1 $^{+}$ Pallidal Neurons Have Distinct Circuit Topology and Function. J. Neurosci. *40*, 7855–7876. https://doi.org/10.1523/JNEUROSCI.0361-20.2020.
88. Sanders, T.H., and Jaeger, D. (2016). Optogenetic stimulation of cortico-subthalamic projections is sufficient to ameliorate bradykinesia in 6-ohda lesioned mice. Neurobiol. Dis. *95*, 225–237. https://doi.org/10.1016/j.nbd.2016.07.021.
89. Schor, J.S., Gonzalez Montalvo, I., Spratt, P.W.E., Brakaj, R.J., Stansil, J.A., Twedell, E.L., Bender, K.J., and Nelson, A.B. (2022). Therapeutic deep brain stimulation disrupts movement-related subthalamic nucleus activity in parkinsonian mice. Elife *11*, e75253. https://doi.org/10.7554/eLife.75253.
90. Tian, J., Yan, Y., Xi, W., Zhou, R., Lou, H., Duan, S., Chen, J.F., and Zhang, B. (2018). Optogenetic Stimulation of GABAergic Neurons in the Globus Pallidus Produces Hyperkinesia. Front. Behav. Neurosci. *12*, 185. https://doi.org/10.3389/fnbeh.2018.00185.
91. Xie, C., Power, J., and Prasad, A.A. (2022). Bidirectional Optogenetic Modulation of the Subthalamic Nucleus in a Rodent Model of Parkinson's Disease. Front. Neurosci. *16*, 848821. https://doi.org/10.3389/fnins.2022.848821.
92. Yoon, H.H., Min, J., Hwang, E., Lee, C.J., Suh, J.-K.F., Hwang, O., and Jeon, S.R. (2016). Optogenetic Inhibition of the Subthalamic Nucleus Reduces Levodopa-Induced Dyskinesias in a Rat Model of Parkinson's Disease. Stereotact. Funct. Neurosurg. *94*, 41–53. https://doi.org/10.1159/000442891.
93. Yoon, H.H., Park, J.H., Kim, Y.H., Min, J., Hwang, E., Lee, C.J., Suh, J.K.F., Hwang, O., and Jeon, S.R. (2014). Optogenetic Inactivation of the Subthalamic Nucleus Improves Forelimb Akinesia in a Rat Model of Parkinson Disease. Neurosurgery *74*, 533–540, discussion 540-1. https://doi.org/10.1227/NEU.0000000000000297.
94. Yu, C., Cassar, I.R., Sambangi, J., and Grill, W.M. (2020). Frequency-Specific Optogenetic Deep Brain Stimulation of Subthalamic Nucleus Improves Parkinsonian Motor Behaviors. J. Neurosci. *40*, 4323–4334. https://doi.org/10.1523/JNEUROSCI.3071-19.2020.
95. Degos, B., Deniau, J.-M., Le Cam, J., Mailly, P., and Maurice, N. (2008). Evidence for a direct subthalamo-cortical loop circuit in the rat. Eur. J. Neurosci. *27*, 2599–2610. https://doi.org/10.1111/j.1460-9568.2008.06229.x.
96. Frankle, W.G., Laruelle, M., and Haber, S.N. (2006). Prefrontal Cortical Projections to the Midbrain in Primates: Evidence for a Sparse Connection. Neuropsychopharmacology *31*, 1627–1636. https://doi.org/10.1038/sj.npp.1300990.
97. Isaacs, B.R., Forstmann, B.U., Temel, Y., and Keuken, M.C. (2018). The Connectivity Fingerprint of the Human Frontal Cortex, Subthalamic Nucleus, and Striatum. Front. Neuroanat. *12*, 60. https://doi.org/10.3389/fnana.2018.00060.
98. Haber, S.N., and Knutson, B. (2010). The Reward Circuit: Linking Primate Anatomy and Human Imaging. Neuropsychopharmacol *35*, 4–26. https://doi.org/10.1038/npp.2009.129.
99. Lazaridis, I., Tzortzi, O., Weglage, M., Märtin, A., Xuan, Y., Parent, M., Johansson, Y., Fuzik, J., Fürth, D., Fenno, L.E., et al. (2019). A hypothalamus-habenula circuit controls aversion. Mol. Psychiatry *24*, 1351–1368. https://doi.org/10.1038/s41380-019-0369-5.
100. Lecca, S., Meye, F.J., Trusel, M., Tchenio, A., Harris, J., Schwarz, M.K., Burdakov, D., Georges, F., and Mameli, M. (2017). Aversive stimuli drive hypothalamus-to-habenula excitation to promote escape behavior. Elife *6*, e30697. https://doi.org/10.7554/eLife.30697.
101. Creed, M., Ntamati, N.R., Chandra, R., Lobo, M.K., and Lüscher, C. (2016). Convergence of Reinforcing and Anhedonic Cocaine Effects in the Ventral Pallidum. Neuron *92*, 214–226. https://doi.org/10.1016/j.neuron.2016.09.001.
102. Itoga, C.A., Berridge, K.C., and Aldridge, J.W. (2016). Ventral pallidal coding of a learned taste aversion. Behav. Brain Res. *300*, 175–183. https://doi.org/10.1016/j.bbr.2015.11.024.
103. Knowland, D., Lilascharoen, V., Pacia, C.P., Shin, S., Wang, E.H.-J., and Lim, B.K. (2017). Distinct Ventral Pallidal Neural Populations Mediate Separate Symptoms of Depression. Cell *170*, 284–297.e18. https://doi.org/10.1016/j.cell.2017.06.015.
104. Saga, Y., Richard, A., Sgambato-Faure, V., Hoshi, E., Tobler, P.N., and Tremblay, L. (2017). Ventral Pallidum Encodes Contextual Information and Controls Aversive Behaviors. Cereb. Cortex *27*, 2528–2543. https://doi.org/10.1093/cercor/bhw107.
105. Vachez, Y.M., and Creed, M.C. (2020). Deep Brain Stimulation of the Subthalamic Nucleus Modulates Reward-Related Behavior: A Systematic Review. Front. Hum. Neurosci. *14*, 578564. https://doi.org/10.3389/fnhum.2020.578564.
106. Wulff, A.B., Tooley, J., Marconi, L.J., and Creed, M.C. (2019). Ventral pallidal modulation of aversion processing. Brain Res. *1713*, 62–69. https://doi.org/10.1016/j.brainres.2018.10.010.
107. Menegas, W., Akiti, K., Amo, R., Uchida, N., and Watabe-Uchida, M. (2018). Dopamine neurons projecting to the posterior striatum reinforce avoidance of threatening stimuli. Nat. Neurosci. *21*, 1421–1430. https://doi.org/10.1038/s41593-018-0222-1.
108. Menegas, W., Bergan, J.F., Ogawa, S.K., Isogai, Y., Umadevi Venkataraju, K., Osten, P., Uchida, N., and Watabe-Uchida, M. (2015). Dopamine neurons projecting to the posterior striatum form an anatomically distinct subclass. Elife *4*, e10032. https://doi.org/10.7554/eLife.10032.
109. Bloem, B.R., Okun, M.S., and Klein, C. (2021). Parkinson's disease. Lancet *397*, 2284–2303. https://doi.org/10.1016/S0140-6736(21)00218-X.
110. Pfeiffer, R.F. (2016). Non-motor symptoms in Parkinson's disease. Parkinsonism Relat. Disord. *22*, S119–S122. https://doi.org/10.1016/j.parkreldis.2015.09.004.
111. Schapira, A.H.V., Chaudhuri, K.R., and Jenner, P. (2017). Non-motor features of Parkinson disease. Nat. Rev. Neurosci. *18*, 435–450. https://doi.org/10.1038/nrn.2017.62.
112. Fasano, A., Romito, L.M., Daniele, A., Piano, C., Zinno, M., Bentivoglio, A.R., and Albanese, A. (2010). Motor and cognitive outcome in patients

with Parkinson's disease 8 years after subthalamic implants. Brain *133*, 2664–2676. https://doi.org/10.1093/brain/awq221.

113. Krack, P., Batir, A., Van Blercom, N., Chabardes, S., Fraix, V., Ardouin, C., Koudsie, A., Limousin, P.D., Benazzouz, A., LeBas, J.F., et al. (2003). Five-Year Follow-up of Bilateral Stimulation of the Subthalamic Nucleus in Advanced Parkinson's Disease. N. Engl. J. Med. *349*, 1925–1934. https://doi.org/10.1056/NEJMoa035275.

114. Limousin, P., Pollak, P., Benazzouz, A., Hoffmann, D., Broussolle, E., Perret, J.E., and Benabid, A.-L. (1995). Bilateral subthalamic nucleus stimulation for severe Parkinson's disease. Mov. Disord. *10*, 672–674. https://doi.org/10.1002/mds.870100523.

115. Péron, J., Frühholz, S., Vérin, M., and Grandjean, D. (2013). Subthalamic nucleus: A key structure for emotional component synchronization in humans. Neurosci. Biobehav. Rev. *37*, 358–373. https://doi.org/10.1016/j.neubiorev.2013.01.001.

116. Temel, Y., Kessels, A., Tan, S., Topdag, A., Boon, P., and Visser-Vandewalle, V. (2006). Behavioural changes after bilateral subthalamic stimulation in advanced Parkinson disease: a systematic review. Parkinsonism Relat. Disord. *12*, 265–272.

117. Tsuboi, T., Wong, J.K., Almeida, L., Hess, C.W., Wagle Shukla, A., Foote, K.D., Okun, M.S., and Ramirez-Zamora, A. (2020). A pooled meta-analysis of GPi and STN deep brain stimulation outcomes for cervical dystonia. J. Neurol. *267*, 1278–1290. https://doi.org/10.1007/s00415-020-09703-9.

118. Zhao, M., Chen, H., Yan, X., Li, J., Lu, C., Cui, B., Huo, W., Cao, S., Guo, H., Liu, S., et al. (2023). Subthalamic deep brain stimulation for primary dystonia: defining an optimal location using the medial subthalamic nucleus border as anatomical reference. Front. Aging Neurosci. *15*, 1187167. https://doi.org/10.3389/fnagi.2023.1187167.

119. Wong, J.K., Viswanathan, V.T., Nozile-Firth, K.S., Eisinger, R.S., Leone, E.L., Desai, A.M., Foote, K.D., Ramirez-Zamora, A., Okun, M.S., and Wagle Shukla, A. (2020). STN Versus GPi Deep Brain Stimulation for Action and Rest Tremor in Parkinson's Disease. Front. Hum. Neurosci. *14*, 578615. https://doi.org/10.3389/fnhum.2020.578615.

120. Welter, M.-L., Schüpbach, M., Czernecki, V., Karachi, C., Fernandez-Vidal, S., Golmard, J.-L., Serra, G., Navarro, S., Welaratne, A., Hartmann, A., et al. (2014). Optimal target localization for subthalamic stimulation in patients with Parkinson disease. Neurology *82*, 1352–1361. https://doi.org/10.1212/WNL.0000000000000315.

121. Chabardes, S., Krack, P., Piallat, B., Bougerol, T., Seigneuret, E., Yelnik, J., Fernandez Vidal, S., David, O., Mallet, L., Benabid, A.-L., and Polosan, M. (2020). Deep brain stimulation of the subthalamic nucleus in obsessive–compulsives disorders: long-term follow-up of an open, prospective, observational cohort. J. Neurol. Neurosurg. Psychiatry *91*, 1349–1356. https://doi.org/10.1136/jnnp-2020-323421.

122. Santin, M.D.N., Tempier, N., Belaid, H., Zenoni, M., Dumas, S., Wallén-Mackenzie, Å., Bardinet, E., Destrieux, C., François, C., and Karachi, C. (2023). Anatomical characterisation of three different psychosurgical targets in the subthalamic area: from the basal ganglia to the limbic system. Brain Struct. Funct. *228*, 1977–1992. https://doi.org/10.1007/s00429-023-02691-2.

123. Wahl, K., Salkovskis, P.M., and Cotter, I. (2008). I wash until it feels right. J. Anxiety Disord. *22*, 143–161. https://doi.org/10.1016/j.janxdis.2007.02.009.

124. Smolinsky, A.N., Bergner, C.L., LaPorte, J.L., and Kalueff, A.V. (2009). Analysis of Grooming Behavior and Its Utility in Studying Animal Stress, Anxiety, and Depression. In Mood and Anxiety Related Phenotypes in Mice, T.D. Gould, ed. (Humana Press), pp. 21–36. https://doi.org/10.1007/978-1-60761-303-9_2.

125. Xue, J., Qian, D., Zhang, B., Yang, J., Li, W., Bao, Y., Qiu, S., Fu, Y., Wang, S., Yuan, T.-F., and Lu, W. (2022). Midbrain dopamine neurons arbiter OCD-like behavior. Proc. Natl. Acad. Sci. USA *119*, e2207545119. https://doi.org/10.1073/pnas.2207545119.

126. Zike, I.D., Chohan, M.O., Kopelman, J.M., Krasnow, E.N., Flicker, D., Nautiyal, K.M., Bubser, M., Kellendonk, C., Jones, C.K., Stanwood, G., et al. (2017). OCD candidate gene *SLC1A1*/EAAT3 impacts basal ganglia-mediated activity and stereotypic behavior. Proc. Natl. Acad. Sci. USA *114*, 5719–5724. https://doi.org/10.1073/pnas.1701736114.

127. Borgius, L., Restrepo, C.E., Leao, R.N., Saleh, N., and Kiehn, O. (2010). A transgenic mouse line for molecular genetic analysis of excitatory glutamatergic neurons. Mol. Cell. Neurosci. *45*, 245–257. https://doi.org/10.1016/j.mcn.2010.06.016.

128. Harris, J.A., Hirokawa, K.E., Sorensen, S.A., Gu, H., Mills, M., Ng, L.L., Bohn, P., Mortrud, M., Ouellette, B., Kidney, J., et al. (2014). Anatomical characterization of Cre driver mice for neural circuit mapping and manipulation. Front. Neural Circuits *8*, 76. https://doi.org/10.3389/fncir.2014.00076.

129. Hippenmeyer, S., Vrieseling, E., Sigrist, M., Portmann, T., Laengle, C., Ladle, D.R., and Arber, S. (2005). A Developmental Switch in the Response of DRG Neurons to ETS Transcription Factor Signaling. PLoS Biol. *3*, e159. https://doi.org/10.1371/journal.pbio.0030159.

130. Dumas, S., and Wallén-Mackenzie, Å. (2019). Developmental Co-expression of Vglut2 and Nurr1 in a Mes-Di-Encephalic Continuum Preceeds Dopamine and Glutamate Neuron Specification. Front. Cell Dev. Biol. *7*, 307. https://doi.org/10.3389/fcell.2019.00307.

131. G. Paxinos, ed. (2009). The Rhesus Monkey Brain: In Stereotaxic Coordinates 2 (Elsevier, Acad. Press).

132. Dupuis, J.P., Feyder, M., Miguelez, C., Garcia, L., Morin, S., Choquet, D., Hosy, E., Bezard, E., Fisone, G., Bioulac, B.H., and Baufreton, J. (2013). Dopamine-Dependent Long-Term Depression at Subthalamo-Nigral Synapses Is Lost in Experimental Parkinsonism. J. Neurosci. *33*, 14331–14341. https://doi.org/10.1523/JNEUROSCI.1681-13.2013.

133. Froux, L., Le Bon-Jego, M., Miguelez, C., Normand, E., Morin, S., Fioramonti, S., Barresi, M., Frick, A., Baufreton, J., and Taupignon, A. (2018). D5 dopamine receptors control glutamatergic AMPA transmission between the motor cortex and subthalamic nucleus. Sci. Rep. *8*, 8858. https://doi.org/10.1038/s41598-018-27195-6.

134. Hogg, S. (1996). A review of the validity and variability of the Elevated Plus-Maze as an animal model of anxiety. Pharmacol. Biochem. Behav. *54*, 21–30. https://doi.org/10.1016/0091-3057(95)02126-4.

135. Lister, R.G. (1987). The use of a plus-maze to measure anxiety in the mouse. Psychopharmacology *92*, 180–185. https://doi.org/10.1007/BF00177912.

STAR★METHODS

KEY RESOURCES TABLE

REAGENT or RESOURCE	SOURCE	IDENTIFIER
Antibodies		
Alexa Fluor 488 AffiniPure Donkey Anti-Chicken IgY (IgG) (H + L) antibody	Jackson ImmunoResearch Labs	Cat#703-545-155; RRID:AB_2340375
Anti-GFP antibody	Abcam	Cat#ab13970; RRID:AB_300798
A594 donkey anti-rabbit antibody	Abcam	Cat#ab150068
Anti-GFP antibody	Aves Lab	Cat#GFP-1010
Anti-RFP antibody	Chromotek	Cat#5f8
Anti-Fluorescein-POD antibody	Roche	Ref. 11426346910
Anti-Digoxigenin-POD antibody	Roche	Ref. 11207733910
Bacterial and Virus Strains		
rAAV2/EF1a-DIO-hChR2(H134R)-eYFP 3.8 × 10^{12} virus molecules/mL	UNC Vector Core, Chapel Hill, NC, USA and Dr. R. Jude Samulski, PhD	N/A; Report Number: R46504
rAAV2/EF1a-DIO-eYFP 4.6 × 10^{12} virus molecules/mL	UNC Vector Core, Chapel Hill, NC, USA and Dr. R. Jude Samulski, PhD	N/A; Report Number: R46503
rgAAV2-hSyn-DIO-EGFP	Addgene, gift from Bryan Roth (http://n2t.net/addgene:50457)	RRID:Addgene_50457
AAV2/5-EF1a-DIO-ChR2(H134R)-mCherry	UNC Vector Core, Chapel Hill, NC, USA	N/A; AV4385E
Chemicals, Peptides, and Recombinant Proteins		
Optibond FL 1 Prime	Kerr	Ref. 25881
Optibond FL 2 Adhesive	Kerr	Ref. 25882
DNQX disodium salt	Bio-Techne	CAT#2312
D-AP5	Bio-Techne	CAT#0106
Biocytin	Sigma-Aldrich	CAT#B4261
Alexa Fluor 647 Streptavidin	Life Technologies	CAT#S21374; RRID:AB2336066
REDExtract-N-Amp	Sigma-Aldrich	CAT#R4775
QIAquick PCR Purification Kit	QIAGEN	CAT#28104
T7 RNA Polymerase (1000u)	PROMEGA	CAT#P2075
T3 RNA Polymerase (1000u)	PROMEGA	CAT#P2083
Recombinant RNasin® Ribonuclease Inhibitor (2,500u)	PROMEGA	CAT#N2511
DIG RNA Labeling Mix	Sigma-Aldrich	CAT#11277073910
10X Fluorescein-RNA Labeling Mix	Sigma-Aldrich	CAT#11685619910
Illustra ProbeQuant G-50 Micro Columns	Sigma-Aldrich	CAT#GE28-9034-08
Denhart's solution (x50)	Sigma-Aldrich	CAT#D2532
Salmon Sperm DNA 10 mg/mL	Sigma-Aldrich	CAT#D7656
Cy3 Mono NHS Ester 10 mg	Sigma-Aldrich	CAT#GEPA13104
NHS-fluorescein (5/6-carboxyfluorescein succinimidyl ester), mixed isomer 100 mg	Thermo Fisher Scientific	CAT#46410
Experimental Models: Organisms/Strains		
Mouse: B6; 129S-Tac1tm1.1(cre)Hze/J	Jackson Laboratories	Jax #021877; RRID:IMSR_JAX:021877
Mouse: B6; 129P2-Pvalb$^{tm1(cre)Arbr}$/J	Jackson Laboratories	Jax #017320; RRID:IMSR_JAX:008069
Mouse: Tg(Slc17a6-icre)1Oki; Vglut2^{Cre}	Ole Kiehn, Copenhagen University, Denmark	N/A; MGI:4881727

(*Continued on next page*)

Continued

REAGENT or RESOURCE	SOURCE	IDENTIFIER
Mouse: Pitx2$^{tm4(cre)Jfm}$	James Martin, University of Texas, USA	N/A; MGI:2445429
Macaque (*Macaca mulatta*) brain block sample	Chantal François,Sorbonne Université, Institut du Cerveau – Paris Brain Institute- ICM, CNRS, APHP, Hôpital de la Pitié Salpêtrière	N/A
Oligonucleotides		
See Table S1		
Recombinant DNA		
Vglut2 Plasmid	SourceBiosciences	N/A; REF: IRAVp968E0467D
Pitx2 Plasmid	SourceBiosciences	N/A; REF: IMAGp998C10933Q
PV Plasmid	SourceBiosciences	N/A; REF: IRAVp968E0480D
Tac1 Plasmid	SourceBiosciences	REF IRCLp5011A095D
hVglut2 Plasmid	Origene: SC126809	CAT#RC210189L4
hPitx2 Plasmid	SourceBiosciences	REF IRATp970D04108D
hPV Plasmid	SourceBiosciences	REF IRCMp5012A0742D
Viaat Plasmid	SourceBiosciences	REF IRAVp968H05111D
Gad2 Plasmid	SourceBiosciences	REF IRAVp968D0750D
Gad1 Plasmid	From Dr Jacques Mallet	N/A
Software and Algorithms		
Ndp2.view software	Hamamatsu	*Cat#SBIS0066E04*
EthoVision XT	Noldus Information Technology, The Netherlands	RRID:SCR_000441
MED-PC	Med Associates inc, Fairfax, USA	RRID:SCR_012156
GraphPad Prism version 7.00 for Windows	GraphPad Software, La Jolla California USA	RRID:SCR_002798
Spike2 software version 7	Cambridge Electronic Design Limited, Cambridge ENGLAND.	RRID:SCR_000903
pClamp 10 (version 10.3 & 10.6)	Molecular Devices	RRID:SCR_011323
QuPath	https://qupath.github.io/	RRID:SCR_018257
Other		
NanoZoomer S60	Hamamatsu	RRID:SCR_022537
Nanozoomer 2.0-HT	Hamamatsu	RRID:SCR_021658
Cryostat: Leica CM1950	Leica	RRID:SCR_018061
Vibratome: Leica VT1200S	Leica	RRID:SCR_018453
Fluoromount-G®	SouthernBiotech	Cat#0100-01
Spatial Place Preference Box	Panlab	Cat#76-0278
Operant conditioning boxes	MED-PC, Med Associates inc	N/A
Picospritzer III	Parker	RRID:SCR_018152
Mono Fiber-optic Cannula	Doric Lenses	Cat#MFC_200/245-0.37_ 5.0mm_ZF1.25_FLT
Splitter Branching Fiber-optic Patch Cords	Doric Lenses	Cat#BFP(2)_200/240/900-0.22_ 1m_FCM-2xZF1.25
1 × 1 Fiber-optic Rotary Joints	Doric Lenses	Cat#FRJ_1 × 1_FC-FC
E600FN, Eclipse workstation	Nikon, Japan	N/A
Nikon Fluor 60 X/1.0 NA	Nikon, Japan	N/A
Nikon Intensilight C-HGFI	Nikon, Japan	N/A
MultiClamp 700B Microelectrode Amplifier	Molecular Devices LLC	RRID:SCR_018455

(*Continued on next page*)

Continued

REAGENT or RESOURCE	SOURCE	IDENTIFIER
Digidata 1550B digitizer	Molecular Devices	N/A
Elipar LED polymerisation lamp	3M Espe	N/A
Arduino UNO Card	Arduino	RRID:SCR_017284

RESOURCE AVAILABILITY

Lead contact

Further information and requests for resources and reagents should be directed to and will be fulfilled by the lead contact, Åsa Wallén-Mackenzie (asa.mackenzie@ebc.uu.se).

Materials availability

This study did not generate new unique reagents.

Data and code availability

- All data reported in this paper will be shared by the lead contact upon request.
- This paper does not report original code.
- Any additional information required to reanalyze the data reported in this paper is available from the lead contact upon request.

EXPERIMENTAL MODEL AND STUDY PARTICIPANT DETAILS

Cre-recombinase mouse strains

Vglut2-Cre[127] (courtesy of Ole Kiehn, Copenhagen University, Denmark), Pitx2-Cre[53,54] (courtesy of James Martin, University of Texas, USA), Tac1-Cre[128] (Jackson Laboratories, B6; 129S-Tac1tm1.1(cre)Hze/J; Jax #021877), PV-Cre[129] (Jackson Laboratories, B6; 129P2-Pvalbtm1(cre)Arbr/J; Jax #017320, common name B6 PV-Cre).

Vglut2-Cre, Pitx2-Cre, Tac1-Cre, PV-Cre transgenic mice were maintained at the local animal facility of Uppsala University before and during behavioral experiments, or at University of Bordeaux (Pitx2-Cre, Vglut2-Cre) for *in vivo* electrophysiological experiments. Mice were maintained on a C57BL/6NTac background, and all breedings were performed *in-house*.

Mice had access to food and water *ad libitum* in standard humidity and temperature conditions and with a 12-h dark/light cycle unless otherwise specified.

PCR analyses were performed on ear biopsies to confirm the Cre-positive genotype (Vglut2-Cre forward, 5′TTG CAT CGC ATT GTC TGA GT AG, reverse; 5′TTC CCA CAC AAG ATA CAG ACT CC, Pitx2-Cre, Tac1-Cre, PV-Cre forward, 5′GCG GTC TGG CAG TAA AAA CTA TC; reverse, 5′GTG AAA CAG CAT TGC TGT CAC TT).

All experimental procedures using mice followed Swedish (Animal Welfare Act SFS 1998:56) and European Union Legislation (Convention ETS 123 and Directive 2010/63/EU), and were approved by local ethical committees in Uppsala and/or Bordeaux (N°50120205-A).

Adult Cre-positive males and females mice were used in all the experiments. Mice that underwent surgery were at lest 8–10 weeks old, and initial experiments were performed at least 4 weeks following viral injection and canula impantation.

Macaque brain tissue

No monkey was sacrificed for this study. Brain tissue from 1 male adult (10 years old) macaque specimen (*Macaca mulatta*) originated from another study[122] and was donated for the current study by Chantal François (Sorbonne Université, Institut du Cerveau – Paris Brain Institute- ICM, CNRS, APHP, Hôpital de la Pitié Salpêtrière), Animal care was carried out in strict accordance with the European Union Directive of 2010 (Council Directive 2010/63/EU) for care and use of laboratory animals. The authorisation for conducting experiments was approved by the Ethics Committee in Animal Experiment Uppsala (agreement no. Ce5/2011/014) and Bordeaux (agreement no. APAFIS#37555) universities. For further details, see Santin et al., 2023.[122]

METHOD DETAILS

Fluorescent *in situ* hybridization (FISH) histochemistry

Mouse brain preparation

To prepare brain sections for mRNA analysis by FISH, brains were quickly dissected from mice euthanized by cervical dislocation, snap-frozen in cold (−30°C to −35°C) 2-methylbutane (≥99%, Honeywell) and kept at −80°C until usage. Coronal serial sections were prepared on a Leica CM1950 Cryostat at 16μm thickness and placed onto Superfrost glass slides in series of 8 slides (Thermo Fischer). Slides prepared for FISH analysis were stored in −80°C until usage.

Macaque brain preparation

The brain was removed from the skull, divided into several blocks, and a block containing the STN area was cut on a cryostat at 16 μm. 300 sections including the whole STN (bregma −9,45; bregma −13,50) were collected, one section per slide. Sections were mounted on slides and stored at −80°C. Slides at the bregma level −11,25 were used in this study.

FISH analysis procedure for detection of mRNA in brain sections

For detection of selected mRNAs in cryosections, mRNA-directed fluorescent riboprobes were prepared from cDNA (Oramacell, Paris). Probes were synthesized by PCR from plasmid (DNA template) containing T3 and T7 promotor sequences using promoter-attached primers to detect: Mouse: Vglut2; Pitx2; Tac1; PV; Gad1; Gad2; Primate: hVglut2; hPitx2; hPV (Tac1 applicable from mouse) (See KRT for a list of PCR primers). Digoxigenin (DIG) and fluorescein-labeled RNA probes were made by a transcriptional reaction with incorporation of DIG or fluorescein labeled nucleotides.[130] Specificity of probes was verified using NCBI blast.

FISH experiments were performed following our previously described protocol.[130] Cryosections were air-dried, fixed in 4% paraformaldehyde and acetylated in 0.25% acetic anhydride/100 mM triethanolamine (pH 8). All sections were treated with two probes to allow analysis of colocalization (co-FISH). Sections were hybridized for 18 h at 65°C in 100 μL of formamide-buffer containing 1 μg/mL digoxigenin-labeled riboprobe (DIG) and 1 μg/mL fluorescein-labeled riboprobe. Sections were washed at 65°C with saline sodium citrate (SSC) buffers of decreasing strength, and blocked with 20% fetal bovine serum and 1% blocking solution. Fluorescein epitopes were detected with horseradish peroxidase (HRP) conjugated anti-fluorescein antibody at 1:5000 and revealed using Cy2-tyramide at 1:250. HRP-activity was stopped by incubation of sections in 0.1 M glycine followed by a 3% H2O2 treatment. DIG epitopes were detected with HRP anti-DIG Fab fragments at 1:1500 and revealed using Cy3 tyramide at 1:100. Nuclear staining was performed with 4′ 6-diamidino-2-phenylindole (DAPI). All slides were scanned at 20x resolution using the Hamamatsu Nanozoomer 2.0-HT Digital slide scanner (Hamamatsu). Laser intensity and time of acquisition were set separately for each riboprobe. Images were analyzed using the NDP.view2 software (Hamamatsu Photonics). Regions of interest were identified according to the Paxinos mouse brain atlas.[60] Positive cells refer to a staining in a cell body clearly above background and surrounding a DAPI-stained nucleus. Colocalization was determined by the presence of the signals for both probes in the soma of the same cell. Tac1 outline was used as PSTN reference and Pitx2 outline was used as STN reference.

Countings

Countings were performed manually using the NDP.view2 and QuPath softwares. Cells were defined by a circle outline (DAPI nuclear staining plus the FISH-generated fluorescent signal), fluorescent signals were checked channel by channel for each selected cell. Intensity, luminosity, contrast parameters were set in the softwares for each probe pair. DAPI (nuclear staining) was used to distinguish if two cells were located close to each other. High and low expression of each probe was analyzed, and countings collected for analysis and comparison.

Mouse: For each probe combination, three sections were analyzed by counting. The region analyzed was the region between bregma −2,03 and −2,27.[60]

Macaque: For each probe combination, one section was analyzed by counting. used The region analyzed was the region at bregma −11,25 mm.[131]

Stereotaxic virus injection and fiber optic probe implantation

Stereotaxic injections were performed in Pitx2-Cre, Vglut2-Cre, PV-Cre, Tac1-Cre mice under isofluorane anesthesia (4% for induction and maintained at 1–1.5% air mix v/v). After being placed in a stereotaxic apparatus, mice received subcutaneous injection of analgesic and anti-inflammatory drugs (buprenorphine, 0.1 mg/kg and Carprofen, 5 mg/kg) as well as a local analgesic (lidocaine, 7 mg/kg) before the incision of the skin. Mice were bilaterally injected in the STN/pSTN with a virus containing either a Cre-dependent Channelrhodopsin (ChR2) construct coupled with an eYFP reporter (rAAV2/EF1a-DIO-hChR2(H134R)-eYFP), or only the eYFP reporter (rAAV2/EF1a-DIO-eYFP), respectively, 3.8×10^{12} virus molecules/mL and 4.6×10^{12} virus molecules/mL (viruses purchased from UNC Vector Core, Chapel Hill, NC, USA) at the following mouse brain coordinates (from Paxinos and Franklin, 2013): anteroposterior (AP) = −1.90 mm, mediolateral (ML) = +/− 1.70 mm from the midline and 250 nL of virus was injected with a NanoFil syringe (World Precision Instruments, Sarasota, FL, USA) at two dorsoventral levels (DV) = −4.65 mm and −4.25 mm from the dura matter at 100 nL.min-1. *Optic cannula implantation*: Optic cannulas (Doric Lenses) were implanted directly after completion of virus injections in mice prepared for behavior analysis. Two skull screws were implanted in the skull to hold the optic cannula-cement-skull complex. Optibond FL Prime 1 and 2 Adhesive (Kerr) were then applied and harden using Elipar LED polymerisation lamp (3M Espe). Optic cannulas were implanted bilaterally above the STN (coordinates: AP = −1.90 mm, ML = +/−1.70 mm from the midline DV = −4.30 mm) or the VP (coordinates: AP = +0.45 mm, ML = +/−1.55 mm from the midline, DV = −4.00 mm), and fixed with dental cement. 1 mL of saline was injected subcutaneously at the end of the surgery.

For *ex vivo* electrophysiology experiments, Vglut2-Cre mice were injected into the LHb and the STN. A glass pipette (30–50 μm tip diameter) filled with rgAAV2-hSyn-DIO-EGFP and was lowered at the LHb coordinates: AP: −1.55 mm; ML: −0.50 mm; DV: −2.65 mm depth and 120 nL were injected using a picospritzer III (Parker). Similarly, a glass pipette filled with AAV2-EF1a-DIO-ChR2(H134R)-mCherry was lowered at the STN coordinates: AP: −1.90 mm; ML: −1.60 mm; DV: −4.65/-4.30 mm and 2 times 120 nL were injected. 5 min after the last injection, the glass pipette was withdrawn. After stitching, mice were transferred to a cage placed on a heating pad until waking up.

Single-cell extracellular recordings

Surgery

In vivo single cell extracellular recordings started after a post-injection recovery period of at least 4 weeks. Mice were anesthetized with a mix isoflurane-air (0.8–1.8% v/v) and placed in a stereotaxic apparatus. Optic fiber, optrode and glass micropipettes coordinates were AP = −1.90 mm, ML = +/− 1.70 mm and DV = −4.30 mm for the STN and AP = −1.60 mm, ML = +/−0.50 mm, DV = −2.00 to −3.30 mm for the LHb.

STN optotagging

A custom-made optrode was made with an optic fiber (100 μm diameter, Thorlabs) connected to a laser (MBL-III-473 nm-100 mW laser, CNI Lasers, Changchun, China) mounted and glued on the recording glass micropipette which was filled with 2% pontamine sky blue in 0.5 μM sodium acetate (tip diameter 1–2 μm, resistance 10–15 MΩ). The distance between the end of the optic fiber and the tip of the recording pipette varied between 650 nm and 950 nm. Extracellular action potentials were recorded and amplified with an Axoclamp-2B and filtered (300 Hz/0.5 kHz). Single extracellular spikes were collected online (CED 1401, SPIKE2; Cambridge Electronic Design). The laser power was measured before starting each experiment using a power meter (PM100D; Thorlabs). The baseline was recorded for 100 s for each neuron before starting any light stimulation protocols which were set and triggered with Spike2 software. Light protocol consisted in a peristimulus time histogram (PSTH, 0.5 Hz, 5 ms pulse duration, 5–8 mW) for at least 100 s followed, after returned to baseline, by a "behavioral" protocol corresponding to the parameters used for behavioral experiments (20 Hz, 5 ms pulse duration, 5–8 mW).

LHb recordings

An optic fiber and a recording pipette filled with either 2% pontamine sky blue or 2% neurobiotin were respectively positioned in the STN and LHb. For each LHb neurons, a PSTH was recorded upon STN optogenetic stimulation (PSTH 0.5 Hz, 5 ms pulses, 5–8 mW) for at least 100 s. Neurons are considered as excited during the PSTH protocol when, following the light pulses centered on 0, the number of spikes/5ms bin is higher than the baseline (−500 ms–0 ms) plus two times the standard deviation. Injection of neurobiotin (2% neurobiotin in 0.5 M acetate sodium) by juxtacellular iontophoresis was performed in some cases for precise spatial identification of excited neurons.

Ex vivo electrophysiology

STN, EP and VP neurons were recorded in acute brain slices, prepared as previously described.[132,133] Briefly, STN^{Pitx2}/CTRL, STN^{Pitx2}/ChR2 and STN^{Vglut2} mice (>12 months) were deeply anesthetized with an i.p. injection of ketamine/xylazine (75/10 mg/kg) mixture and then perfused *trans*-cardially with ice-cold (0°C–4°C) modified artificial cerebrospinal fluid (ACSF), equilibrated with 95% O_2 and 5% CO_2, and containing (in mM): 230 sucrose, 26 $NaHCO_3$, 2.5 KCl, 1.25 NaH_2PO_4, 0.5 $CaCl_2$, 10 $MgSO_4$ and 10 glucose. (pH∼7,35). The brain was quickly removed, glued to the stage of a Leica VT1200S vibratome (Leica, Germany), immersed in the ice-cold ACSF and sectioned into 300 μm thick parasagittal slices. Slices containing the LHb, the STN and the VP/EP were then incubated for 1 h to a standard oxygenated ACSF solution, warmed (∼35°C) containing (in mM unless otherwise stated): 126 NaCl, 26 $NaHCO_3$, 2.5 KCl, 1.25 NaH_2PO_4, 2 $CaCl_2$, 2 $MgSO_4$, 10 glucose, 1 sodium pyruvate and 4.9 μML-gluthathione reduced. Single slices were then transferred to a recording chamber at room temperature 22°C–26°C and perfused continuously with oxygenated ACSF.

Electrophysiological recordings

Patch-clamp recordings were performed under infrared gradient contrast video microscopy on an upright microscope (E600FN, Eclipse workstation, Nikon, Japan) equipped with a 60× water-immersion objective (Nikon Fluor 60×/1.0 NA). The microscope was also equipped with epifluorescence (Nikon Intensilight C-HGFI) allowing visualization of STN neurons expressing the ChR2-mCherry as well as LHb-projecting EP and VP neurons retrogradely labeled with GFP, respectively.

STN, VP and EP neurons were recorded using low-resistance pipettes (impedance, 3–8 MΩ) prepared from borosilicate glass capillaries (GC150F10; Warner Instruments, Hamden, CT, USA) with a horizontal puller (P- 97; Sutter Instruments, Novato, CA, USA). In voltage-clamp experiments, the internal solution contained the following (in mM): 135 K-gluconate, 3.8 NaCl, 1 $MgCl_2.6H_2O$, 10 HEPES, 0.1 EGTA, 0.4 Na_2GTP, 2 $Mg_{1.5}ATP$, 5 QX-314 and 5.4 biocytin (pH = 7.2, ∼292 mOsm). Data were acquired using a Multiclamp 700B amplifier connected to a Digidata 1550B digitizer controlled by Clampex 10.3 (Molecular Devices, Sunnyvale, CA, USA). Acquisitions were performed at 20 kHz and low-pass filtered at 4 kHz. Series resistance was monitored throughout the experiment by voltage steps of −5 mV. Data were discarded when the series resistance changed by >20%. Biocytin-filled neurons were identified.

For optogenetic stimulation, a LED laser source (Prizmatix, Israel) connected to optic fiber (∅: 500 μm) was placed above the brain slice. Light intensities ranged from 4mW to 90 mW at the tip of the optic fiber depending of the type experiments. For cell body stimulation, continuous 100 ms long duration light stimulation (λ = 470nm) was applied at low (4mW) and high (90 mW) intensities. To evoke synaptic transmission, single pulses or train of stimulation (800 pulses at 20Hz) of 1ms duration at full power (90 mW) were used in order to maximize axon terminal depolarization and efficient release of neurotransmitter. The magnitude of EPSCs was examined in whole-cell voltage-clamp mode at a holding potential of −60 mV. Junction potential (∼13 mV) was not corrected. EPSC latencies were calculated as the difference between the time of the pulse and the beginning of the negative deflection of the EPSC. After electrophysiological recordings, slices were fixed overnight in 4% paraformaldehyde, and maintained in PBS-azide at 0.2% at 4°C until immunohistochemical processing.

Pharmacology

Unless otherwise stated, all pharmaceutical substances were prepared in distilled water as concentrated stock solutions and stored at −20°C. On the day of the experiment, the substances were diluted and applied through the bath perfusion system. In some experiments glutamatergic antagonists were used to demonstrate that the recorded EPSCs from STN inputs were mediated by AMPA/Kainate and MNDA receptors. NMDA receptors were blocked with 50 μM D-(−)-2-amino-5-phosphonopentanoic acid (D-APV). AMPA/kainate receptors with 20 μM 6,7-dinitroquinoxaline-2,3-dione (DNQX disodium salt).

Behavioral testing

Following a post-surgical recovery period of approximately four weeks, mice were analyzed in a battery of behavioral tests. Throughout, the following stimulation protocol was used: 473 nm light, 5 mW, 20 Hz, 5 ms pulse delivered by an MBL-III-473 nm-100 mW laser (CNI Lasers, Changchun, China). Duration and condition of stimulation are specified for each test. After completed behavioral tests, mice were sacrificed and brains analyzed histologically and for assessment of optic cannula position (see below for details). The initial sample size was determined based on previous published studies with similar experimental design.

Habituation

Three weeks after surgery and before the first behavioral test, all mice were handled and habituated to the experimental room and to the optic cables to reduce the stress during the day of the experiment. Before each behavioral test, mice were acclimatized for 30 min in the experimental room.

Opto-Open Field

Mice were individually placed in neutral cages for 3 min in order to recover after connecting the optic cables. Mice were subsequently placed in the central zone of the open field arena and allowed to freely explore it for 5 min before starting the test. The open-field chamber consisted in a 50 cm, squared, transparent, plastic arena with a white floor. The Opto-Open Field test consisted of a 20-min session divided into 5-min alternating time intervals (OFF-ON-OFF-ON). Each 5-min interval was then divided into two 2.5-min intervals for analysis. The patch cable was connected to a rotary joint, which was attached on the other end to a laser that was controlled by an Arduino Uno card (Arduino). During the light-ON trials, blue light was delivered according to the behavioral stimulation protocol (20Hz, 5ms, 5mW). Self-grooming and escape behaviors were manually recorded by an experimenter blind to the experimental groups using the EthoVision XT 14.0 tracking software (Noldus Information Technology, The Netherlands).

Opto-RT-CPP

A three-compartment apparatus (Spatial Place Preference Box, Panlab, Harvard Apparatus) was used for the Opto-RT-CPP test. The apparatus is composed of two compartments with different visual and tactile cues for both floors and walls and a connecting corridor (neutral compartment) with transparent walls and floor. The study was carried out throughout 8 consecutive days preceded by one *"Habituation"* day. On each day of the experiment, subjects were placed in a neutral cage for at least 3 min to recover after connecting the optic cables. Mice were subsequently moved into the transparent corridor of the apparatus where, after 30–50 s, the doors were removed and animals allowed to freely explore the apparatus. The position of the mouse was detected by a camera positioned above the apparatus. On *"Habituation"*, *"Pre Test"* and "*Conditioning Place Test"* days (15 min), mice were connected to the optic fiber but no light was paired to any chamber. On the "*Real Time Conditioning"* days (30 min), one chamber was randomly chosen as a light-paired chamber (counterbalanced across animals) while the other one was subsequently assigned as light-paired chamber on the "*Reverse Real Time Conditioning"* days (30 min). Every time the subject entered the light-paired chamber, the laser was activated according to the stimulation protocol (20Hz, 5ms, 5mW). Cumulative duration of the time spent in each compartment was recorded by using the Ethovision XT13.0/14.0 tracking software (Noldus Information Technology, The Netherlands). Mice that showed strong initial preference during the "Pre-Test" for either one of the two compartments (<25% or >75% of time spent) were excluded from the statistical analysis.

Opto-Avoidance-EPM

This test was carried out inside a classic EPM apparatus. This has the shape of a plus, made of two open and two closed arms (35 cm length) with walls (15 cm high) and crossed in the middle to create a center platform, elevated 50 cm from the floor. The two open and exposed arms provide a naturally aversive space that mice avoid to spend time in. The two other arms are enclosed by walls on three sides, providing a sheltered space than mice prefer over the open and naturally aversive arms. The center area is less exposed than the open arms, but not sheltered. In a standard EPM test, mice prefer the closed arms and avoid the open arms and center.[134,135]

The re-designed version of the EPM test aims to assess the aversive effect induced by the photostimulation in comparison to the natural aversion experienced in the open arms of the apparatus. Mice were first connected to the optic fiber then placed in a neutral cage for 5 min to recover from cable connection. Mice were next placed individually in the center of the maze facing one of the open arms and allowed to freely explore the apparatus for 15 min. In the Opto-Avoidance-EPM test, photostimulation was activated upon entry into any of the closed arms, and disabled by leaving it. In contrast, visiting the open arms or occupying the center zone had no effect on photostimulation. The tip of the nose was used as a reference for the activation of optogenetic stimulation and for detecting the position of the animal inside the apparatus. In this way the animal had complete control over the stimulation so that only the voluntary entry into one of the two closed arms resulted in optogenetic stimulation. Likewise, it was only the position of the head (nose) that determined which compartment of the EPM apparatus was occupied by the animal. Thus, by pairing the sheltered area with optogenetic activation, the Opto-Avoidance-EPM protocol allows direct comparison between a naturally aversive context (open arm) and effect caused by subthalamic activation (closed arm). Time spent in each compartment and number of entries were recorded with a

camera placed above the EMP arena and data analyzed by the Ethovision XT13.0/14.0 tracking software (Noldus Information Technology, The Netherlands).

Opto-negative reinforcement paradigm (Opto-NR)

Mice response was assessed by using operant conditioning boxes equipped with two nose-poke devices (MED-PC, Med Associates inc, Fairfax, USA) and laser for optogenetic stimulation. One device was defined as active, which when activated terminates the optogenetic stimulation schedule, while the other one was demarcated as inactive, which had no control over the laser. The presentation of the optogenetic stimulations (10 s) were alternated with variable-time intervals, when no stimulation was applied. An active nose-poke (FR1) at any point during this pre-stimulation interval or during the stimulation epoch itself terminates the optogenetic stimulation schedule and produces a visible safety signal (house light ON) that marks a period of safety.

Sugar positive reinforcement paradigm (Sugar-PR)

Under this protocol mice learned to make active nosepokes to receive sugar pellets. The experiment is carried out during several consecutive sessions (30 min; 1 session/day). Mice were food restricted by administering one daily feeding of 2.5- 3g of standard food following each daily session.

Training and testing took place in operant boxes (MED-PC, Med Associates inc, Fairfax, USA) interfaced with lasers for optogenetic stimulation and equipped with nosepoke (NP) devices on each side of a food dispenser. One NP device was designated as active and marked by a light while the device on the other side of the dispenser was selected as inactive. Nose-poking to the active NP carried out when the light is on (''delivering phase''), names as ''Active delivering NPs'', resulted in a cue tone presentation (0.5s), a 20 mg sucrose pellet delivery (5TUT, TestDiet, St. Louis, USA) and/or laser activation for optogenetic stimulation (20Hz, 5ms, 5mW) according to the different phases of the task, while nose-poking to the inactive side resulted in no cues presentation, sugar delivery and/or laser activation. During 20s that follows a sugar pellet delivery and/or optogenetic stimulation the visual cue for the active NP goes off (''no delivering phase'') and active nose-poking during this period did not result in auditory cue presentation, sugar delivery and/or laser activation. Active NPs carried out during this period were registered as ''Active no delivering NPs'' and summed to the ''Active delivering NPs'' to obtain the total Active NPs. Nose pokes in the inactive hole, did not activate the sugar dispenser, the laser and the acoustic cue at any time but they were registered as ''Inactive delivering NPs'' when carried out during the ''delivering phase'' and as ''Inactive no delivering NPs'' when performed during the ''no delivering phase''. ''Inactive no delivering NPs'' were summed to the ''Inactive delivering NPs'' to obtain the total Inactive NPs.

Phase 1 (Acquisition phase): Sugar was delivered in response to an Active delivering NPs. This phase lasts until the animal acquires a stable sugar SA rate, which consists of at least 10 received sugar pellet/session with a <20% variation during three consecutive days. Animal that did not acquired a stable sugar SA rate within the third week were excluded from the experiment.

Phase 2 (Sugar-Stimulation phase): Optogenetic stimulation (10 s stimulation 20Hz, 5ms, 5mW) was delivered as a consequence of an active delivering NPs simultaneously to the activation of the sugar dispenser. This phase lasts 5 consecutive sessions (1 session/day).

Phase 3: Depending on the response upon pairing sugar delivering and optogenetic stimulation mice were exposed either to an ''only sugar'' or to an ''only stimulation'' phase 3. In the case of a reduction in the number of active NPs, and in order to exclude that such response was not due to a loss of interest for sugar, the subsequent and last phase is characterized ''sugar reinstatement'' during the following phase 3, restoring the same conditions previously applied during phase 1. If NP activity was similar or higher during phase 2 compared to phase 1 mice were moved to the ''only stimulation'' phase 3 (5 sessions) in order to assess whether optogenetic stimulation alone was sufficient to maintain a comparable NP activity.

Phase 4: Depending on the response upon ''only stimulation'' phase 3 mice were exposed either to an ''only sugar'' phase 4 or to an ''only cues'' phase 4. In the case of extinction of the active response, the subsequent and last phase 4 (2 sessions) was characterized by ''sugar reinstatement'' restoring the same conditions previously applied during phase 1. If NP activity was not affected during phase 3 compared to phase 2 mice were moved to the ''only cue'' phase 4 (3 sessions) where mice were only exposed to visual and auditory cues previously accompanied with sugar and optogenetic stimulation.

Phase 5: Response extinction was finally asses in a last phase (3 sessions) in which active NP activity was followed by no sugar delivery, no optogenetic stimulation and no cues presentation.

Criteria for exclusion from the analysis

Mice were excluded from individual test analysis if.

1. In the Opto-Open Field they jumped out of the arena during photostimulation so that the analysis of other parameters was made impossible (n = 5).
2. In the Opto-RT-CPP if, during the pre-test (Day 1), there was a strong initial preference, such that the time spent in a compartment exceeded 80% of the total, or a strong avoidance, so that the time spent in a compartment was less than 20% of the total (n = 4).
3. During Sugar-PR if they have not acquired a stable rate of self-sugaring, which consisted of at least 10 sugar lozenges received/session with <20% variation during three consecutive days (n = 8) or if they have done more than 30 active nose-pokes in a short time during the initial sessions of the paradigm (n = 4).

Mice were excluded from all analyzes if post-hoc histological examination revealed insufficient viral expression or when both cannulas trajectory resulted to be not close enough to the site of interest (n = 8). Mice were excluded if histological analysis was not possible due to premature death of the animal or if the animal had to be sacrificed for health reasons during the study (n = 6). In case of loss of the optical assembly during the study, only the data acquired up to that moment were included. In case incorrect genotype was revealed during post-hoc analysis (n = 2).

Post-injection histological analysis

Following behavioral analyses, recombinase mice were deeply anesthetized and perfused *trans*-cardially with phosphate-buffer-saline (PBS) followed by ice-cold 4% formaldehyde. Brains were extracted and 60 μm or 40 μm sections were cut with a Leica VT1200S vibratome or a Leica CM1950 Cryostat after being put in sucrose scale and frozen at −80° freezer, respectively.

Fluorescent immunohistochemistry was performed to enhance the YFP signal. All mice were analyzed. Mice that displayed strong cellular YFP labeling in the expected area (STN or pSTN) and in which optic cannulas trajectory could be estimated as positioned above the area of interest were included in the statistical analyses of the electrophysiological and behavioral experiments.

After rinsing in PBS, sections were incubated for 3 h in a blocking solution made of PBS containing 0.3% X-100 Triton and 5% normal donkey serum, followed by incubation with primary antibodies diluted in the blocking solution, overnight at 4°C (chicken anti-GFP 1:1000, cat. no. ab13970, Abcam). Next day, sections were rinsed in PBS and incubated for 2 h with secondary antibodies diluted in PBS containing 0.3% X-100 Triton and 5% normal donkey serum (A488 donkey anti-chicken 1:1000, cat. no. 703–545-155, Jackson ImmunoResearch). After rinsing in PBS, sections were incubated for 10 min with DAPI diluted in distilled water (1:5000). Sections were mounted with Fluoromount-G mounting medium (SouthernBiotech) and cover-slipped. Analysis was performed upon slide scanning using the Hamamatsu NanoZoomer S60 Digital slide scanner (Hamamatsu) scanner followed by visualization using the NDPView2 software (Hamamatsu).

QUANTIFICATION AND STATISTICAL ANALYSIS

For behavioral analysis, to compare two or more groups across two or more treatments or time points, repeated measures two-way ANOVA followed by Šídák or Tukey multiple comparisons were performed. For analysis of 2 groups, paired t test or Mann Whitney test were performed when appropriate. For single cell extracellular recordings, Friedman test was performed to compare three matched groups followed by Dunn's multiple comparisons. All graph plotting and statistical analysis were performed using GraphPad Prism (version 7.00 for Windows, GraphPad Software, La Jolla California USA). Data are expressed on the plots as means ± SEM. For all datasets, significance was defined by a p value of <0.05. The following were used: * $p < 0.05$; ** $p < 0.01$; *** $p < 0.001$. All statistical tests, the exact value of n and what n represents are reported in the figure legends and Supplemental file 1. Number of male and females used in each experiment are reported in Supplemental file 1.